nature communications

Article

https://doi.org/10.1038/s41467-024-52672-0

Arid, mosaic environments during the Plio-Pleistocene transition and early hominin dispersals in northern Africa

Received: 5 March 2024

Accepted: 18 September 2024

Published online: 04 October 2024

Check for updates

Iván Ramírez-Pedraza[1,2,3] ✉, Carlos Tornero[1,4], Hassan Aouraghe[5], Florent Rivals[1,2,6], Robert Patalano[3,7], Hamid Haddoumi[5], Isabel Expósito[1,2], Antonio Rodríguez-Hidalgo[1,8], Steffen Mischke[9], Jan van der Made[10], Pedro Piñero[1,2], Hugues-Alexandre Blain[1,2], Patrick Roberts[3,11,12], Deepak Kumar Jha[11], Jordi Agustí[1,2,6], Christian Sánchez-Bandera[1,2], Abdelkhalek Lemjidi[13], Alfonso Benito-Calvo[14], Elena Moreno-Ribas[1,2], Aïcha Oujaa[13], Hicham Mhamdi[5], Mohamed Souhir[5], Al Mahdi Aissa[5], M. Gema Chacón[1,2,15] & Robert Sala-Ramos[1,2]

The earliest archaeological evidence from northern Africa dates to *ca.* 2.44 Ma. Nevertheless, the palaeoenvironmental setting of hominins living in this part of the continent at the Plio-Pleistocene transition remains poorly documented, particularly in comparison to eastern and southern Africa. The Guefaït-4 fossil site in eastern Morocco sheds light on our knowledge of palaeoenvironments in northern Africa. Our study reveals the oldest known presence of C_4 plants in the northern part of the continent in a mosaic landscape that includes open grasslands, forested areas, wetlands, and seasonal aridity. This diverse landscape and resource availability likely facilitated the occupation of the region by mammals, including potentially hominins. Our regional-scale study provides a complementary perspective to global-scale studies and highlights the importance of considering the diversity of microhabitats within a given region when studying species-dispersal dynamics.

Reconstructing past environments is critical to understanding the ecological dynamics of mammalian, including early hominin, occupation of regions within and beyond Africa. While the landscape of the Plio-Pleistocene transition has been extensively studied in eastern[1–8], central[9,10], and southern Africa[2,11–14], there is a notable knowledge gap for the northern African region. The presence of sites with hominin-associated artefacts in Algeria[15,16] and Morocco[17,18] during the Early Pleistocene, dating to as early as 2.44 Ma, has put a spotlight on northern Africa for investigating hominin evolution and dispersals. Nevertheless, detailed insights

[1]Institut Català de Paleoecologia Humana i Evolució Social (IPHES-CERCA), Tarragona, Spain. [2]Departament d'Història i Història de l'Art, Universitat Rovira i Virgili (URV), Tarragona, Spain. [3]isoTROPIC Research Group, Max Planck Institute of Geoanthropology, Jena, Germany. [4]Department of Prehistory, Autonomous University of Barcelona (UAB), Bellaterra, Spain. [5]Faculté des Sciences, Département de Géologie, Université Mohammed Premier, Oujda, Morocco. [6]Institució Catalana de Recerca i Estudis Avançats (ICREA), Barcelona, Spain. [7]Department of Biological and Biomedical Sciences, School of Health and Behavioral Sciences, Bryant University, Smithfield, USA. [8]Consejo Superior de Investigaciones Científicas, Instituto de Arqueología (CSIC-Junta de Extremadura), Mérida, Spain. [9]Institute of Earth Sciences, University of Iceland, Reykjavík, Iceland. [10]Consejo Superior de Investigaciones Científicas (CSIC), Museo Nacional de Ciencias Naturales, Departamento de Paleobiología, Madrid, Spain. [11]Department of Archaeology, Max Planck Institute of Geoanthropology, Jena, Germany. [12]School of Archaeology, University of Philippines, Diliman, Quezon City, Philippines. [13]Institut National des Sciences de l'Archéologie et du Patrimoine (INSAP), Rabat, Morocco. [14]Centro Nacional de Investigación Sobre la Evolución Humana (CENIEH), Burgos, Spain. [15]UMR 7194-Histoire Naturelle de l'Homme Préhistorique (MNHN/CNRS/UPVD), Paris, France. ✉e-mail: ramirezpedrazaivan@gmail.com

into the palaeoenvironment of this region at that time remain sorely lacking.

The area presently occupied by the Sahara Desert has experienced, for over 8 Myr, short-lived (~8–14 kyr) periods of greening[19], known as Green Sahara Periods (GSPs), that have facilitated the dispersal of diverse animal species[19,20]. Large-scale global studies have established the picture of a gradual shift towards a drier climate and greater environmental variability in the transition from the Pliocene to the Pleistocene, influenced by the Northern Hemisphere Glaciation[21–24]. However, the impact of these global-scale climate shifts on regional ecosystems and biodiversity is unclear[25]. Regional-scale studies provide critical, complementary perspectives to global models, where opposing local trends and a diversity of microhabitats in the same region can be explored[26].

We present palaeoecological proxy information from the Guefaït-4.2 (GFT-4.2; 34° 13′ 3.4″ N, 2° 24′ 13.2″ W) fossil locality in eastern Morocco, dated close to the Plio-Pleistocene transition[27] (Fig. 1; Supplementary Note 1 and Supplementary Fig. 1–3). GFT-4.2 was excavated with a trench of 28 m², revealing a 180 cm sequence formed by a palustrine event, in which more than 3000 large vertebrate remains were buried. Taphonomic study indicates a time-averaged fossil assemblage formed relatively quickly (in geological terms), consistent with the palaeomagnetic, stratigraphic, and biochronological data (Supplementary Note 1). We utilised bulk and sequential enamel stable carbon ($\delta^{13}C$) and oxygen ($\delta^{18}O$) isotope analysis, stable carbon isotope analysis from plant wax *n*-alkanes, dental microwear and mesowear analyses, and analyses of small vertebrates, pollen, micro-crustaceans and algae to provide on-site ecological evidence. Our approach aims to offer a holistic landscape reconstruction using the distinct palaeoenvironmental perspectives and varying temporal and spatial resolutions each proxy provides (Supplementary Note 2 and Supplementary Tables 1 and 2). We produce insights into the environmental conditions prevailing in northwestern Africa at the time of the documented presence of early hominins in the region.

Results

Stable isotope analysis of large vertebrate tooth enamel

$\delta^{13}C$ values indicate a dominance of C_3 plant consumption (trees, woody shrubs, bushes, herbs and temperate grasses) by mammals ($\delta^{13}C$ range = −13.3‰ to −1.4‰; median = −9‰; n = 172; Figs. 2 and 3). However, abundant consumption of C_4 plants (likely tropical grasses, shrubs and sedges) is reported in some sampled taxa. *Hipparion* sensu lato (n = 61; range = −11.3 to −1.4‰; median = −7.3‰) and Tragelaphini (n = 42; range = −11.6 to −3.9‰; median = −9.2‰) display the greatest

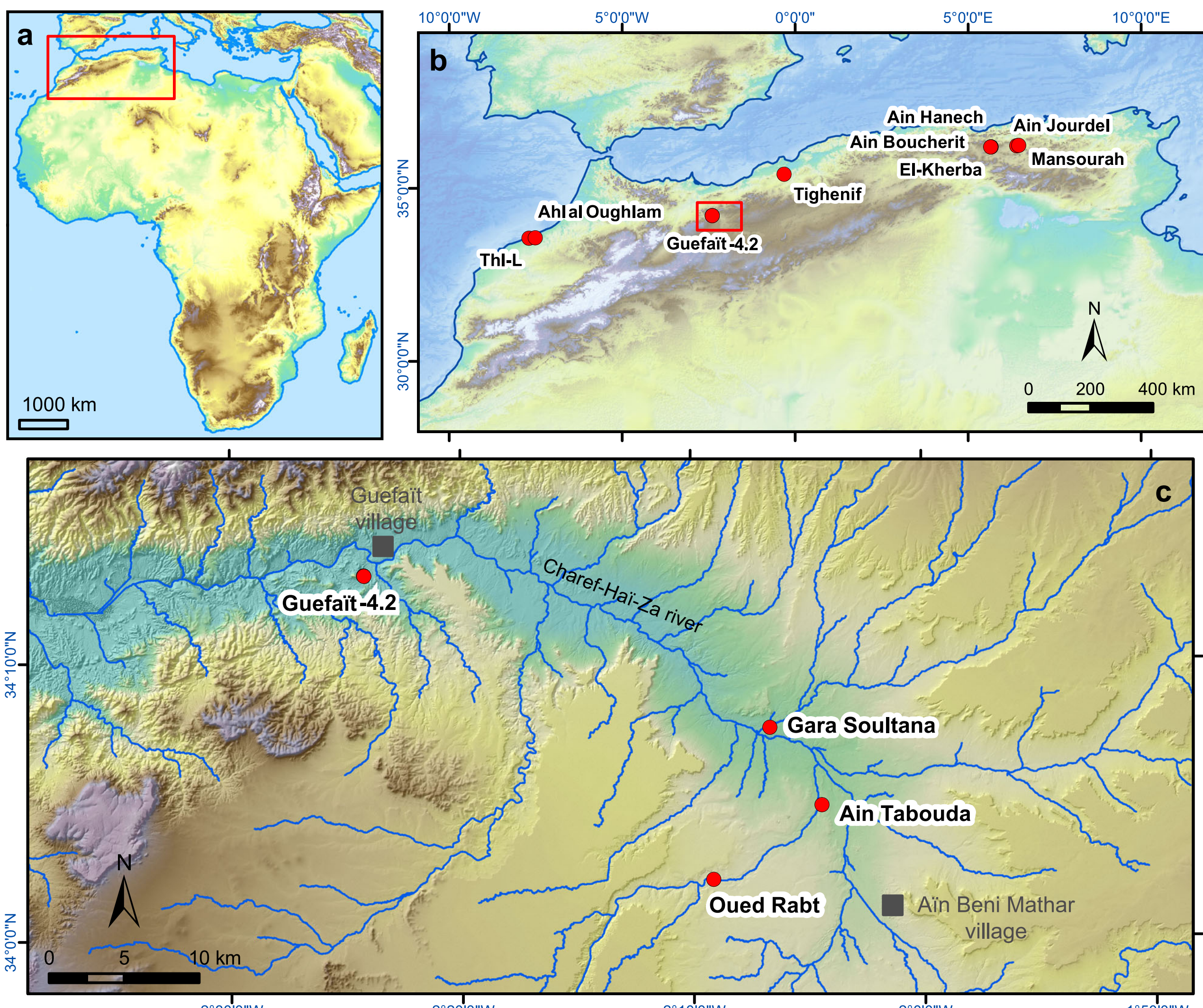

Fig. 1 | Archaeological and palaeontological sites. a Context of the study area in Africa. **b** Early Pleistocene (Thomas Quarry I–Unit L (ThI-L), Tighennif, El-Kherba, Ain Hanech, Mansourah and Ain Boucherit) and Plio-Pleistocene transition (Ahl al Oughlam, Ain Jourdel and Guefaït-4.2) sites of Morocco and Algeria. **c** Position of Guefaït-4.2 and other study area sites attributed to Early Pleistocene (Gara Soultana and Aïn Tabouda) and Middle Pleistocene (Oued Rabt).

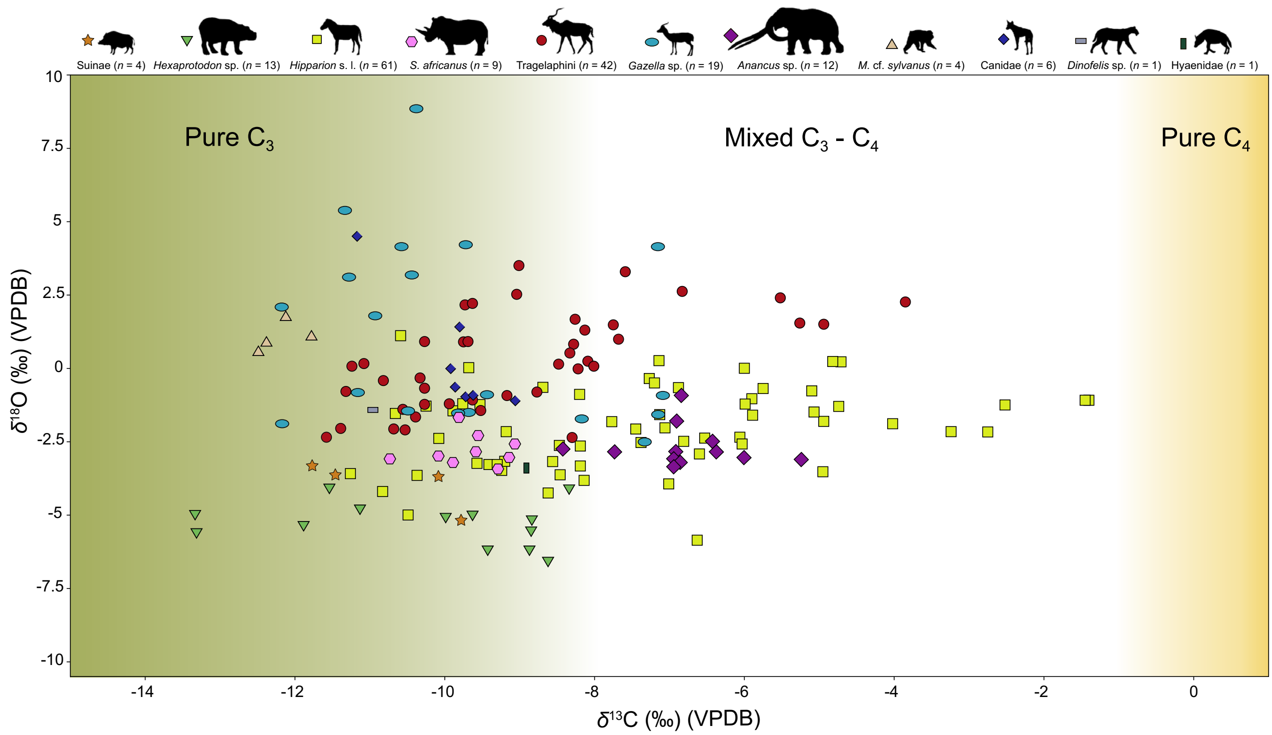

Fig. 2 | The δ^{13}C and δ^{18}O values from the tooth enamel of fossil fauna from GFT-4.2. The isotopic data for *M.* cf. *sylvanus* have been previously published in ref. 28. Each point corresponds to a tooth enamel sample with a total of 168. Silhouettes from PhyloPic (http://phylopic.org). Tragelaphini, Suinae, *S. africanus*, *Dinofelis* sp., and Hyaenidae are under the public domain. Canidae (by Sam Fraser-Smith, vectorised by T. Michael Keesey), *M.* cf. *sylvanus* (by Kai R. Caspar), *Hexaprotodon* sp. and *Hipparion* s. l. (by Zimices), and *Gazella* sp. (by Rebecca Groom) are licensed under Attribution 3.0 Unported (https://creativecommons.org/licenses/by/3.0/). *Anancus* sp. (by Henry Fairfield Osborn, vectorised by Zimices) is licensed under Attribution-ShareAlike 3.0 Unported (https://creativecommons.org/licenses/by-sa/3.0/). Source data are provided as a Source Data file.

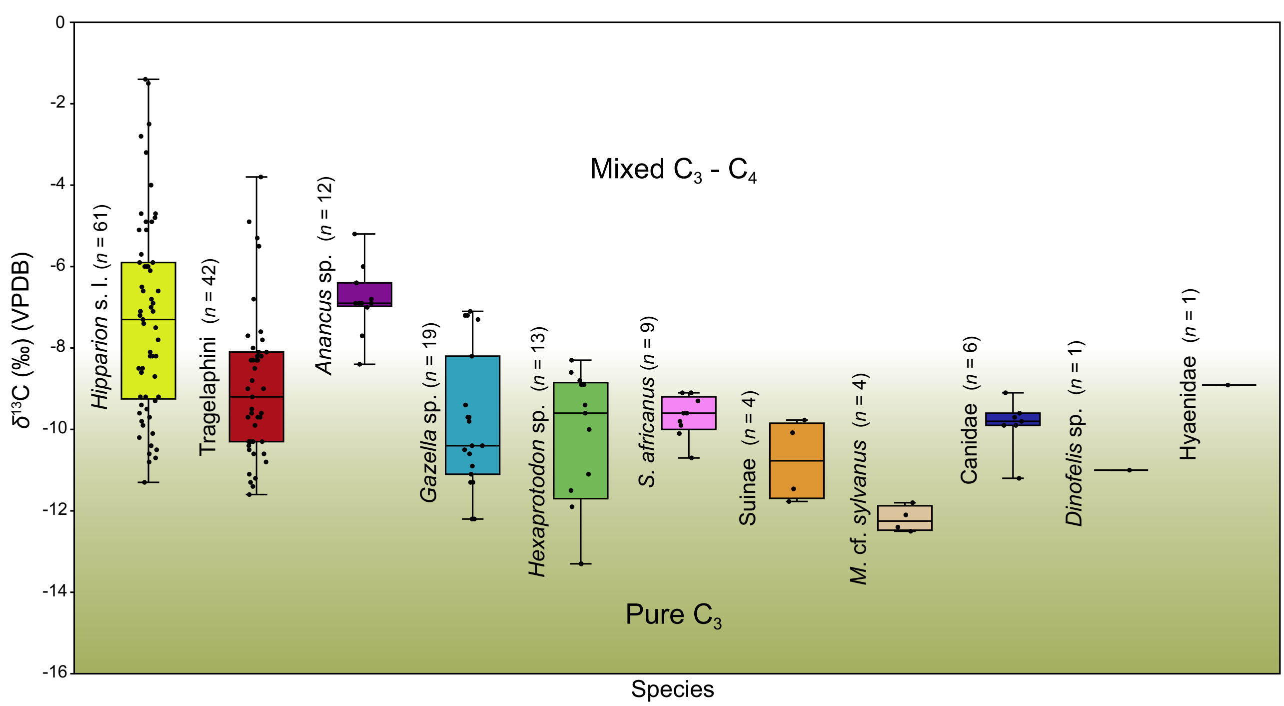

Fig. 3 | Jitter boxplots of δ^{13}C values of fossil fauna from GFT-4.2. Boxes represent the interquartile range (IQR), defined by the 25th (Q1) and 75th (Q3) percentiles, with the median value indicated by a line within the box. Whiskers extend from the box to the minimum and maximum values within 1.5 times the IQR from the quartiles, while data points outside this range are considered outliers. Error bars show the standard deviation (SD). Each point corresponds to a tooth enamel sample. Source data are provided as a Source Data file.

https://doi.org/10.1038/s41467-024-52672-0

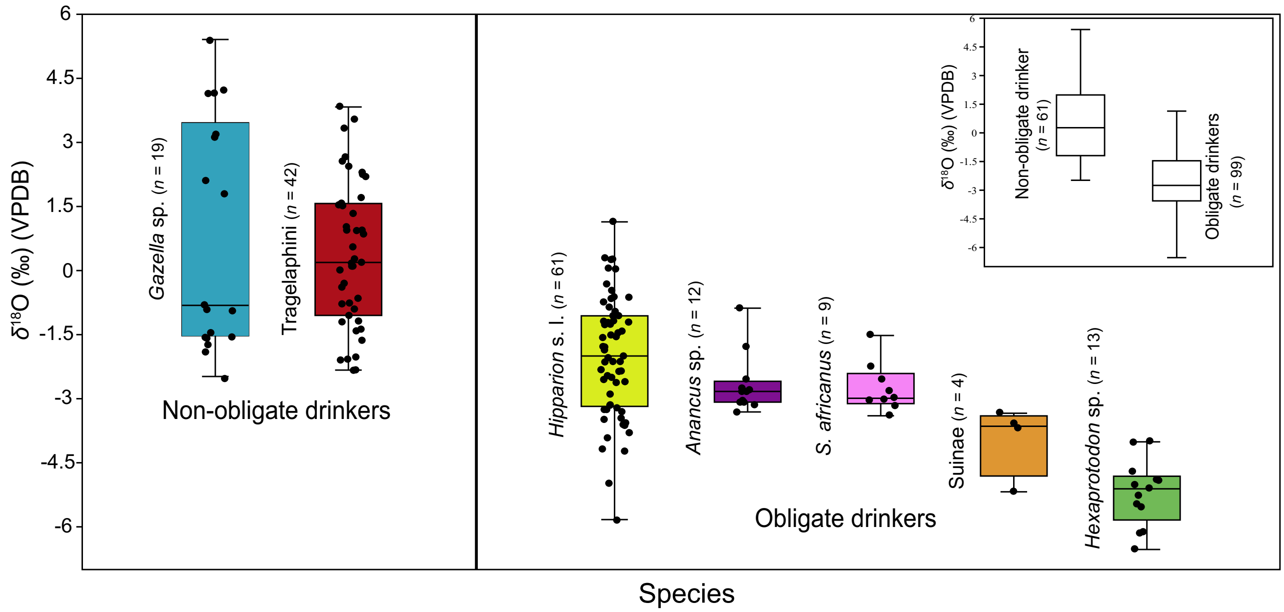

Fig. 4 | Jitter boxplots of $\delta^{18}O$ values for non-obligate and obligate drinking taxa from GFT-4.2. Boxes represent the interquartile range (IQR), defined by the 25th (Q1) and 75th (Q3) percentiles, with the median value indicated by a line within the box. Whiskers extend from the box to the minimum and maximum values within 1.5 times the IQR from the quartiles, while data points outside this range are considered outliers. Error bars show the standard deviation (SD). Each point corresponds to a tooth enamel sample. The boxplots in the upper right corner correspond to all $\delta^{18}O$ values of taxa grouped as non-obligate drinkers (*Gazella* sp. and Tragelaphini) and obligate drinkers (*Hexaprotodon* sp., Suinae, *S. africanus*, *Anancus* sp., and *Hipparion* s. l.). Source data are provided as a Source Data file.

variability in $\delta^{13}C$ values, including the highest values within the assemblage. *Gazella* sp. ($n = 19$; range = −12.2 to −7.1‰; median = −10.4‰) and *Anancus* sp. ($n = 12$; range = −8.4 to −5.2‰; median = −6.9‰) exhibit mixed C_3 and C_4 values, with focus towards a C_3 plant-based diet. *Stephanorhinus africanus* ($n = 9$; range = −10.8 to −9.1‰; median = −9.6 ‰), Suinae ($n = 4$; range = −11.8 to −9.8‰; median = 10.8‰), *Hexaprotodon* sp. ($n = 13$; range = −13.3 to −8.6‰; median = −9.6‰), and *Macaca* cf. *sylvanus* ($n = 4$; range = −12.5 to −11.8‰; median = 12.3‰[28]) exhibit exclusive C_3 plant consumption, with the latter two species presenting the lowest values of the assemblage. The $\delta^{13}C$ values observed in carnivorans reflect those of their prey[29–31]. In the case of GFT-4.2, all carnivorans including the Canidae ($n = 6$; range = −11.2 to −9.1‰; median = −9.8‰), *Dinofelis* sp. ($n = 1$; −11‰), and Hyaenidae ($n = 1$; −8.9‰) were consuming animals with a C_3 plant-based diets.

The $\delta^{18}O$ values of all animal samples ($n = 172$; Fig. 2) measured from GFT-4.2 range from −6.5‰ to 8.8‰ with a median of −1.5‰. *Gazella* sp. ($n = 19$; range = −2.5 to 8.8‰; median = −0.8‰) exhibits the highest $\delta^{18}O$ values in the assemblage, followed by Tragelaphini ($n = 42$; range = −2.3 to 3.8‰; median = 0.2 ‰), Canidae ($n = 6$; range = −1.1 to 4.5‰; median = −0.6‰), and *M.* cf. *sylvanus* ($n = 4$; range = 0.6 to 1.8‰; median = 1‰[28]), which also have values towards the higher end of the spectrum. *Hexaprotodon* sp. ($n = 13$; range = −6.5 to −4‰; median = −5.1‰) shows the lowest $\delta^{18}O$ values of any taxon, followed, in this order, by Suinae ($n = 4$; range = −5.1 to −3.3‰; median = −3.6‰), *S. africanus* ($n = 9$; range = −3.4 to −1.5‰; median = −3‰), *Anancus* sp. ($n = 12$; range = −3.3 to −0.9‰; median = −2.8‰), and *Hipparion* s. l. ($n = 61$; range = −5 to 1.1‰; median = −2‰). Unlike Canidae, the other two carnivores, *Dinofelis* sp. ($n = 1$; −1.4‰) and Hyaenidae ($n = 1$; −3.4‰), have $\delta^{18}O$ values towards the lower end of the overall range. The complete dataset of bulk $\delta^{13}C$ and $\delta^{18}O$ values of mammalian teeth ($n = 170$) is presented in Fig. 2 and described in Supplementary Data 1.

The difference in $\delta^{18}O$ values between non-obligate and obligate drinkers is a proxy for estimated palaeoaridity[32–37]. This difference in GFT-4.2 is 3‰ (obligate drinker mean: −2.5‰, non-obligate drinker mean: 0.5 ‰; Fig. 4 and Supplementary Note 3). The results have been compared to the difference between non-obligate and obligate drinkers in Laikipia (1.7‰) and Tsavo (2.2‰) in Kenya, defined as semi-arid savannas[5,38]. We also compare our data to results from fossil fauna remains from the Ahl al Oughlam site (1.9‰; Supplementary Note 3), penecontemporaneous to GFT-4.2, located in western Morocco, and defined as a dry environment[39]. Our findings show a greater difference between non-obligate and obligate drinkers GFT-4.2 compared to both the current savannas of Laikipia and Tsavo and the fossil site of Ahl al Oughlam, indicating a more arid environment.

For the intra-tooth sequences of $\delta^{13}C$ and $\delta^{18}O$ values, we analysed eight teeth of *Hipparion* s. l., comprising 180 intra-tooth enamel samples (Fig. 5 and Supplementary Data 2). Lower $\delta^{18}O$ values are associated with the cold/wet season, while higher values correspond to the warm/dry season. For $\delta^{13}C$, values above −8‰ would indicate the consumption of C_4 plants. We observed two distinct trends in the sampled teeth of this taxon. In the first (samples in Fig. 5a–e), the $\delta^{13}C$ and $\delta^{18}O$ values exhibit the same seasonal oscillation, with higher consumption of C_4 plants during the warmer/drier season. In the case of one sample in Fig. 5a, the dominant consumption of C_3 plants extended throughout the entire year, while in one sample in Fig. 5b, this pattern occurred with the consumption of C_4 plants. However, in the second trend (samples in Fig. 5g, h), an inverse relationship between $\delta^{18}O$ and $\delta^{13}C$ maximum and minimum values was observed, indicating a greater consumption of C_4 plants during the colder season. This inverse relationship between $\delta^{18}O$ and $\delta^{13}C$ may be associated with the altitudinal mobility of *Hipparion* s. l., indicating a higher consumption of C_3 plants in the highlands during the warm/dry season and a higher consumption of C_4 plants in the lowlands during the cold/wet season. This aligns with the fact that GFT-4.2 is in a mountainous region with altitudes ranging from 600 to 1700 metres. The sample in Fig. 5f shows a progressive increase in the consumption of C_4 plants without a clear correlation with $\delta^{18}O$ values.

The cross-correlations analysis showed a significant relationship between intra-tooth $\delta^{13}C$ and $\delta^{18}O$ in seven of the eight samples (Supplementary Table 3 and Supplementary Fig. 4). The sample without

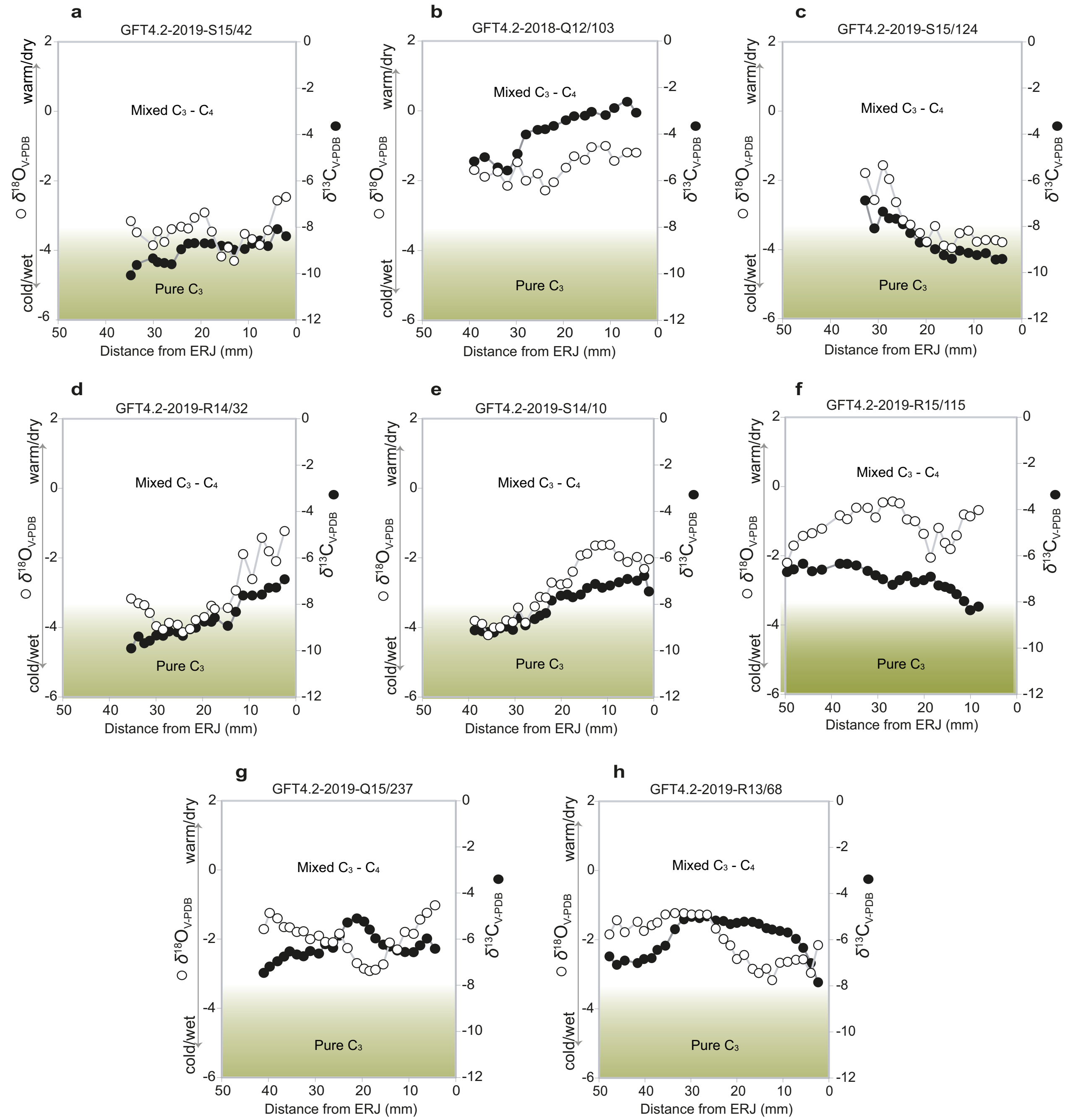

Fig. 5 | Sequential analysis of carbon and oxygen values of bioapatite enamel from *Hipparion* s. l. of GFT-4.2. **a** Sample GFT4.2-2019-S15/42. **b** Sample GFT4.2-2018-Q12/103. **c** Sample GFT4.2-2019-S15/124. **d** Sample GFT4.2-2019-R14/32. **e** Sample GFT4.2-2019-S14/10. **f** Sample GFT4.2-2019-R15/115. **g** Sample GFT4.2-2019-Q15/237. **h** Sample GFT4.2-2019-R13/68. ERJ enamel-root junction. Source data are provided as a Source Data file.

correlation is GFT4.2-2019-R15/115 (Fig. 5f). Among the seven specimens with significant correlation, two (Fig. 5g, h) are negatively correlated, while five display positive cross-correlation coefficients (Fig. 5a–e).

Dental wear

The mesowear analysis measures the relief and sharpness of worn cusp apices on occlusal surfaces, ranging from sharp cusps and high relief (indicative of low abrasion and high attrition) to low relief with rounded cusps (indicative of high abrasion and low attrition). The mesowear scores (MWS) of the three analysed taxa from GFT-4.2 show a narrow range of MWS median values, from 1.4 to 3.1 (Fig. 6 and Supplementary Data 3). These MWS indicate low levels of abrasion for *Gazella* sp. (MWS = 1.4) and Tragelaphini (MWS = 1.9), suggesting a mixed feeding dietary trait dominated by leaf and fruit browsing. In *Hipparion* s. l., despite the MWS being 3.1, there is a high degree of variability among samples, indicating a wide range of dietary abrasiveness, ranging from browse-dominated mixed feeders to pure grazers.

The microwear analysis classifies the extinct taxa along a continuum of dietary abrasiveness, ranging from pure browsers to pure grazers, including mixed feeders, based on the average number of pits and scratches (Fig. 7 and Supplementary Data 3). The *Hipparion* s. l. and the two Bovidae exhibit browse-dominated dietary traits, whereas

 https://doi.org/10.1038/s41467-024-52672-0

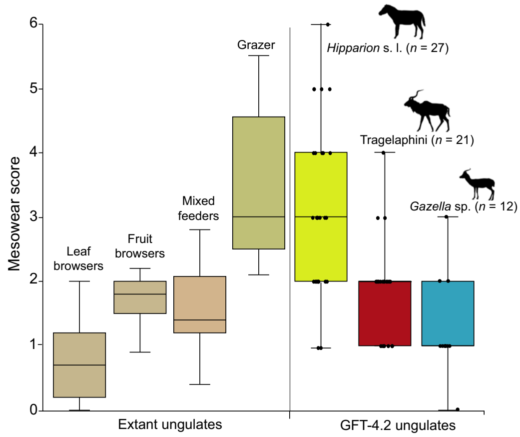

Fig. 6 | Boxplot with mesowear scores (MWS) of the ungulates from GFT-4.2. Boxes represent the interquartile range (IQR), defined by the 25th (Q1) and 75th (Q3) percentiles, with the median value indicated by a line within the box. Whiskers extend from the box to the minimum and maximum values within 1.5 times the IQR from the quartiles, while data points outside this range are considered outliers. Error bars show the standard deviation (SD). Each point corresponds to a tooth enamel sample. Extant ungulates database[129]. Silhouettes from PhyloPic (http://phylopic.org). Tragelaphini under the public domain, *Hipparion* s. l. (by Zimices) and *Gazella* sp. (by Rebecca Groom) are licensed under Attribution 3.0 Unported (https://creativecommons.org/licenses/by/3.0/). Source data are provided as a Source Data file.

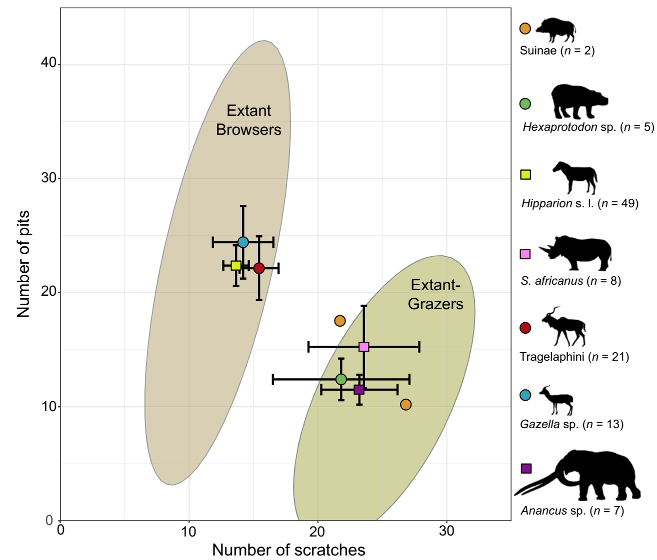

Fig. 7 | Bivariate plot of the average numbers of pits and scratches for the species from GFT-4.2. Error bars correspond to standard deviation (±1 SD) for the fossil samples. Plain ellipses correspond to the Gaussian confidence ellipses ($p = 0.95$). Extant ungulates based on the database[112]. Silhouettes from PhyloPic (http://phylopic.org). Tragelaphini, Suinae and *S. africanus* are under the public domain. *Hexaprotodon* sp. and *Hipparion* s. l. (by Zimices), and *Gazella* sp. (by Rebecca Groom) are licensed under Attribution 3.0 Unported (https://creativecommons.org/licenses/by/3.0/). *Anancus* sp. (by Henry Fairfield Osborn, vectorised by Zimices) is licensed under Attribution-ShareAlike 3.0 Unported (https://creativecommons.org/licenses/by-sa/3.0/). Source data are provided as a Source Data file.

Hexaprotodon sp., *S. africanus*, and Suinae show grass-dominated traits, with *Anancus* sp. exhibiting a pure grass-feeding pattern (Fig. 7). As with mesowear, microwear results reveal a wide range of diets, ranging from browse-dominated mixed feeders to pure grazers. Species in the browsing feeding space (*Hipparion* s. l. and the two Bovidae) have a higher number of pits and a lower number of scratches. By contrast, species in the grazer feeding space (*Hexaprotodon* sp., *S. africanus* and Suinae) have a lower number of pits and a higher number of scratches. *Anancus* sp. is placed among the extant pure grazers because it has the lowest number of pits (11.5). All taxa, except Suinae, exhibit puncture pits.

Plant wax biomarkers

Odd-numbered, long-chain (i.e., C_{27}-C_{31}) lengths dominate the *n*-alkane biomarker distributions in plants and sediments. Of the ten samples analysed, all but one have C_{31} as the dominant *n*-alkane, with the C_{29} and C_{27} alkanes being the second and third most abundant compounds, respectively (Supplementary Note 4 and Supplementary Data 4). The relative abundances of the C_{25} and C_{27} *n*-alkanes are highly correlated (Spearman's correlation, $r_s = 0.89$, $p = 0.007$), as are the relative abundances of C_{29} and C_{31} (Spearman's correlation, $r_s = 0.98$, $p \leq 0.001$), indicating that C_{25}, C_{27}, C_{29} and C_{31} were synthesised by multiple plant-life forms[40,41]. Furthermore, C_{25} and C_{27} co-vary in opposite directions to that of C_{29} and C_{31} throughout the sequence (Fig. 8), suggesting that both submerged or emergent and terrestrial plants contributed biomarkers to the investigated sediments. The average chain length (ACL_{21-33}) ranges from 26.8 to 29.7 (28.2 ± 0.3, $n = 10$), consistent with previous measurements of modern ACL from African terrestrial plants[42–46]. The carbon preference index (CPI) of the C_{21}-C_{33} *n*-alkanes ranges between 2.3 and 10 (5.6 ± 0.9, $n = 8$). These values are typical of plant-derived CPI values[47–50] and indicate no significant plant wax degradation occurred[51,52]. The aquatic plant ratio (P_{aq})[53] ranges between 0.0 and 0.6, while the submerged/terrestrial ratio (STR)[54] ranges between 0.0 and 0.31, trending with the P_{aq} values (Fig. 8).

The $\delta^{13}C$ data from the C_{25}-C_{31} *n*-alkanes further show that there are differences between the C_{25} and C_{27} *n*-alkanes and C_{29} and C_{31} (Student's *t*-test two-tailed (*t*-test) $p \leq 0.0001$; Mann–Whitney *U* test (MWU) $p \leq 0.0001$; Fig. 8). $\delta^{13}C$ values range between −31.5‰ and −28.0‰ (−29.4 ± 1.0‰, $n = 36$) and, when separated by *n*-alkane homologue, between −29.7‰ and −28‰ (C_{25}, −28.6 ± 0.5‰, $n = 9$), −29.8‰, and −28.2‰ (C_{27}, −28.6 ± 0.5‰, $n = 9$), −30.3‰ and −29.4‰ (C_{29}, −29.8 ± 0.3‰, $n = 9$), and −31.5‰ and −29.5‰ (C_{31}, −30.5 ± 0.8‰, $n = 9$). These $\delta^{13}C$ data suggest a C_3-dominated environment. There is a roughly 2.0‰ mean difference between C_{31} and both C_{25} (*t*-test, $p \leq 0.0001$; MWU, $p \leq 0.0001$) and C_{27} (*t*-test, $p \leq 0.0001$; MWU, $p = 0.0001$), with the largest variation of 3.2‰ (GFT 10) between C_{31} and C_{25} and of 3.1‰ (GFT 5) between C_{31} and C_{27}. Additionally, the mean difference between C_{29} and both C_{25} (*t*-test, $p = 0.0001$; MWU, $p = 0.001$) and C_{27} (*t*-test, $p \leq 0.0001$; MWU, $p = 0.001$) is 1.2‰, with the largest variation between C_{29} and C_{25} being 1.8‰ (GFT 1 and 10) and between C_{29} and C_{27} being 1.9‰ (GFT 1). On the other hand, C_{29} and C_{31} differ on average by only 0.8‰ (*t*-test, $p = 0.03$; MWU, $p = 0.1$), and C_{25} and C_{27} differ on average by only 0.2‰ (*t*-test, $p = 1$; MWU, $p = 0.719$). This suggests that the plant-wax input into GFT-4.2 sediments is characterised by two groups; one source contributing predominantly C_{25} and C_{27} *n*-alkanes, and the other contributing C_{29} and C_{31} *n*-alkanes.

Pollen analysis

Concentrations of pollen, spores and other palynomorphs are low throughout the sequence (22.1–286.8 palynomorphs per gram of dry sediment). Tree cover is suggested in four samples by the presence of pine (*Pinus* sp.) and evergreen oak (*Quercus ilex-coccifera* type) and the occasional presence of alder (*Alnus*). Shrub vegetation is not represented, due to the scarce pollen dispersion of these taxa. Herbaceous vegetation is represented by wild grasses (Poaceae), Asteraceae (Tubuliflorae and Liguliflorae types), Amaranthaceae, Apiaceae and Fabaceae (Supplementary Fig. 5 and Supplementary Data 5).

Non-pollen palynomorphs (NPP) include mainly fungal spores such as *Polyporisporites*, *Polyadosporites*, *Glomus* sp., *Exesisporites* and

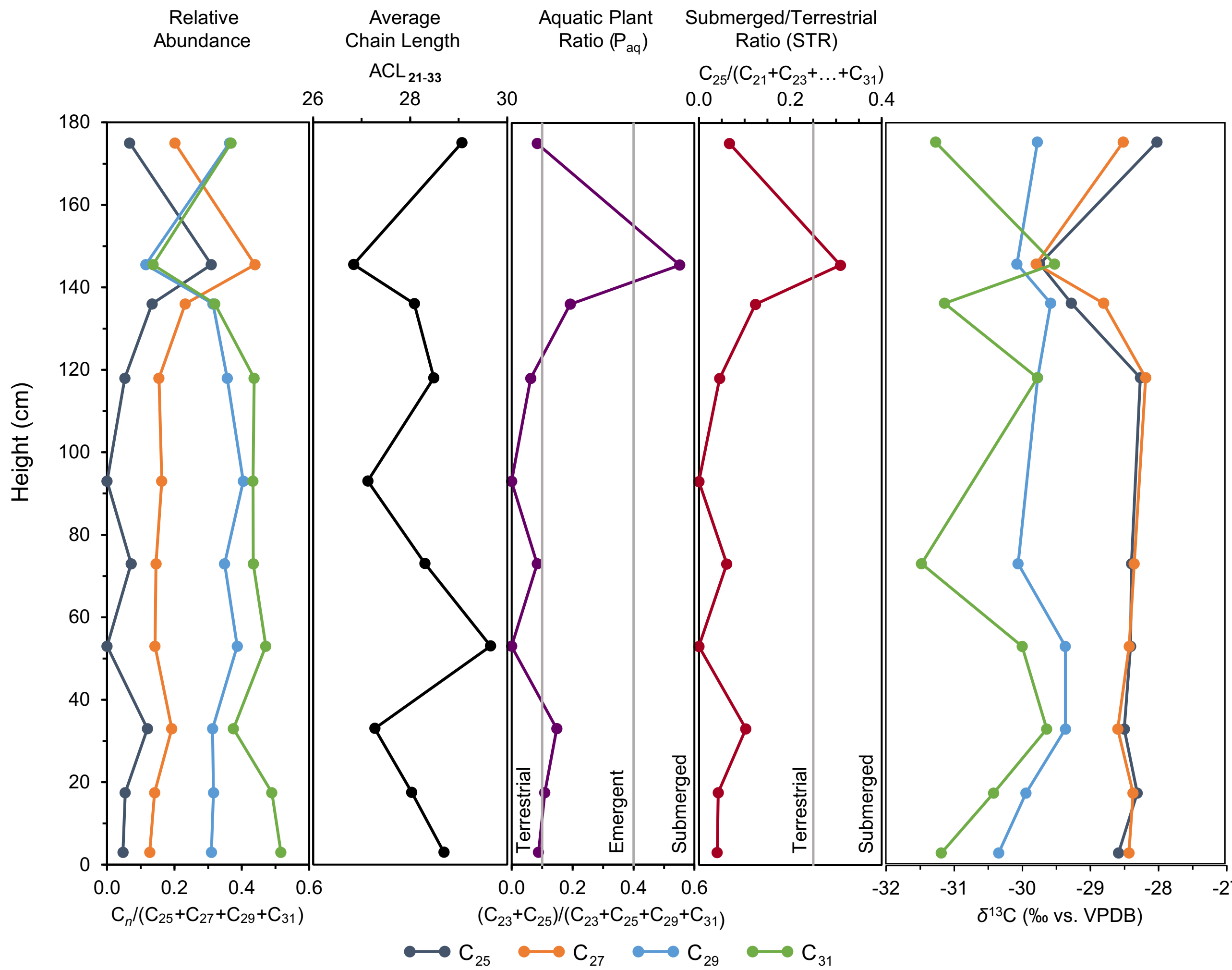

Fig. 8 | Isotopic and biomarker signatures of GFT-4.2 plant wax *n*-alkanes. See "Methods" for ACL calculation. Submerged or floating aquatic plants tend to have STR values greater than 0.25, whereas for the Aquatic Plant Ratio (Paq), aquatic plants tend to have values greater than 0.7, and values ranging between 0.1 and 0.7 typically represent a mixed input of terrestrial, emergent and submerged aquatic plants. The percentages of compound abundances are relative to the dominant *n*-alkanes ($C_{25} + C_{27} + C_{29} + C_{31}$). Higher values reflect relatively increased inputs of the respective compounds. Source data are provided as a Source Data file.

hyphae. Trilete spores from mosses or ferns have also been identified. Other palynomorphs identified (HdV 303 or "protists") have an undetermined ecological origin or are linked to chitin remains of insects and mites (HdV 52[55]). Additionally, microcharcoal concentrations are low, ranging from 18.4 to 157.9 particles per gram (Supplementary Fig. 5).

Small vertebrates

The rodent assemblage is composed of four murine species (*Paraethomys pusillus*, *Paraethomys chikeri*, *Golunda aouraghei*, and *Praomys* cf. *skouri*), two gerbils (Gerbillidae indet. 1, Gerbillidae indet. 2), a ctenodactyline (*Irhoudia* sp.), a sciurid (*Atlantoxerus* sp.), and a glirid (*Eliomys* sp.) (Supplementary Note 5 and Supplementary Fig. 6). The herpetofaunal assemblage includes an anuran (Anura indet., an alytid or ranid frog), a lizard (Lacertidae indet.), an anguid lizard (*Ophisaurus* sensu lato), and two snakes (Natricidae/Elapidae indet. and Colubridae/Lamprophiidae indet.) (Supplementary Note 4 and Supplementary Fig. 7).

Micro-crustaceans and algae remains

The sediment samples from the GFT-4.2 section yielded ostracod valves and algae remains (Supplementary Fig. 8 and Supplementary Note 6). The recorded ostracod taxa comprise *Ilyocypris* sp., *Cypridopsis vidua*, *Neglecandona neglecta*, *Cyprideis torosa*, *Potamocypris* sp., *Heterocypris salina*, *Herpetocypris* sp., *Cypris pubera*, and *Psychrodromus* sp. (ordered by decreasing abundance). Additionally, green macroalgae represented by gyrogonites from three distinct charophyte species occur in two samples, with one sample including as many as 217 gyrogonites per 100 g.

Discussion

Our transdisciplinary, multiproxy approach demonstrates a high degree of habitat variability and environmental heterogeneity at Guefaït-4.2 at the time of the Plio-Pleistocene transition. Wetlands are evidenced by the presence of emergent and submerged plants, as suggested by plant wax biomarkers, non-pollen palynomorphs, and taxa such as ranid or alytid frog indicate a permanent water source. Micro-crustaceans and green algae taxa indicate the presence of a shallow, mostly fresh to slightly brackish water body with a dense aquatic plant cover on the floor. Living hippopotami need to submerge in water, and *Hexaprotodon* sp. suggests a water depth that was never less than 1.5 m. The geological and stratigraphical context of GFT-4.2, characterised by clays, marls and palustrine limestones, including local conglomerates and sandstones[56,57], also supports the presence of water bodies. Meanwhile, tree pollen, dental microwear of species with a leaf-browsing diet, and species like *M.* cf. *sylvanus*, *P.* cf. *skouri*, and

Ophisaurus s. l[58]. indicate the presence of woodlands and humid environments. Additionally, previous studies on the GFT-4.2 macaques link their ecology to the presence of trees[28]. The presence of puncture pits in most large vertebrates suggests the consumption of hard objects, such as fruits or seeds[59,60]. Open grasslands are identified through wild grass pollen and mammalian taxa with a grazing diet (C_3 and C_4 grasses). Some small-vertebrate taxa in the assemblage are also characteristic of open grassy ecosystems, such as *G. aouraghei*[61], and indeed most of the heliophilic reptiles, and *Irhoudia* sp. and *Eliomys* sp. exhibit a preference for rocky habitats[62,63].

This environmental mosaic is further highlighted by the isotopic data. The δ^{13}C values in plant waxes and large vertebrates indicate a predominance of C_3 plants in the region. However, *Hipparion* s. l., Tragelaphini, *Anancus* sp., and *Gazella* sp. also consumed C_4 plants (grasses, sedges or woody shrubs), which may be due to their ability to move over greater distances and select their food. Aridity and warm temperatures are evidenced by the presence of C_4 plants[64]. The significant differences in δ^{18}O values between obligate and non-obligate drinkers corroborate the hypothesis of lower rainfall totals. Additionally, the sequential isotopic analysis performed on *Hipparion* s. l. shows some individuals with marked seasonal aridity, with higher consumption of C_4 plants during the warm/dry season, while others exhibit a diet associated with seasonal altitudinal mobility. Some species are associated with arid conditions, such as gundis (*Irhoudia* sp.[65]), ground squirrels (*Atlantoxerus* sp.[66,67]), *G. aouraghei* and the giant tortoise (*Centrochelys*). Also, changes in the abundance of microcharcoals in the sediments suggest the proliferation of natural forest fires during arid periods[68]. This combination of proxies reveals the important role of temperature and precipitation seasonality in the region.

Together our proxy data demonstrate that the overall environmental context in GFT-4.2 and its surroundings was highly ecotonal. A permanent water body was likely fed by streams or rivers draining the neighbouring highlands, and these were probably surrounded by either forests with overlapping canopies or woodlands with canopies that did not overlap extensively. The riparian woodland would have then transitioned into a wooded grassland that contained stretches of grasses and other herbs and only scattered woody plants. There was likely another structural change toward an open grassland with woody species only occurring in specialised microhabitats that were dependent on water availability. Finally, these lowland dry grasslands would have transformed into montane forests at higher elevations. Climatically, the region was probably generally warm with very arid summers and potentially even semi-desertic conditions, with the vegetation structure dictated by periodic fluctuations in water availability due to seasonal droughts.

It is important to note the varying temporal and spatial scales of our proxies when considering the reconstructed landscape diversity (Supplementary Table 1 and Supplementary Note 2). Pollen and plant waxes can be transported over long distances by various factors, providing reconstructions of the wider region. For example, evidence of forest reconstructed by these proxies at GFT-4.2 could be a riparian forest or woodland in the immediate vicinity of the site or a more distant (e.g., high-altitude) representation. It is also important to note that the production of pollen and waxy compounds varies with plant type and species[48,69], meaning that certain habitats will be over- or under-represented. Meanwhile, our dental wear and stable isotope results are heavily influenced by the dietary preferences of the sampled large vertebrate taxa, with grazers, for example, finding patches of forage in landscapes even where grassland areas are limited[7]. This complicates predicting the extent of these grasslands, something further exacerbated by the fact that these taxa can range widely. However, having several taxa of small and large vertebrates in GFT-4.2 and applying multiple proxy approaches in the same sequence (Supplementary Fig. 2) makes the ecological reconstruction more robust. Indeed, the various scales of these proxies are also a strength, further highlighting the environmental diversity experienced on local and regional scales.

The diet of some taxa in GFT-4.2 provides the oldest known evidence of significant consumption of C_4 plants by large herbivores in northern Africa, especially by *Hipparion* s. l. C_4 plants are virtually absent during the Late Pliocene and Early Pleistocene in Europe[70,71] and northern Africa[39,72,73], and their presence in GFT-4.2 opens up the possibility of an ecosystem not previously considered in these latitudes, contributing to the regional habitat heterogeneity at a time that coincides with the earliest hominin occupations in northern Africa. To date, the oldest hominin occupation is found in Algeria at the Aïn Boucherit site (2.44 Ma[74]; Fig. 1b), which has a chronology slightly younger than GFT-4.2 and is also located in the Intra-Atlas Maghrebian Depression[56]. In addition, the Aïn Beni Mathar–Guefaït Basin (Fig. 1c) is rich in archaeological sites like the Early Pleistocene sites of Aïn Tabouda and Gara Soultana with Mode 1 lithic tools, or the Middle Pleistocene site of Oued Rabt with Mode 2 lithic tools[18]. This reinforces the likely continuous presence of hominins in the region in which our site is located.

C_4 plants constituted a significant component of the diet and habitat of several early hominins during the Late Pliocene and Early Pleistocene in eastern and southern Africa[8,75–77]. Even in Central Africa, 3000 km from the Rift Valley, the diet of *Australopithecus bahrelghazali* from Koro Toro in Chad (3.5 Ma[78]) was dominated by the consumption of C_4 plants[9]. Nevertheless, the C_4 open dry grasslands and shrublands were only one component of these hominin-occupied landscapes. The presence of C_4 plants was part of a mosaic ecosystem comprising a great diversity of resources, including wetlands and savannas[9,79,80], as is also the case of GFT-4.2. In contrast to some classical theories linking hominins to specific habitats[81–83], recent studies in eastern Africa provide evidence for the important role of climate and habitat variability in hominin evolution[26,84–86]. Additionally, increased ecological resource variability is considered a major factor in species' adaptive versatility[80,87–89].

The aridity observed in GFT-4.2 is consistent with the global trend towards progressive aridification during the Plio-Pleistocene transition[22,24]. The period from ~2.7 to 2.55 Ma coincides with the presence of East African Rift System paleolake periods[19,90] and seven Green Sahara Periods[19], which could have created significant green corridors connecting eastern and northern Africa. However, the regional landscape complexity presented in GFT-4.2 can only be fully understood through terrestrial context studies, preferably on-site, complementing those conducted at a global scale in marine records. The Aïn Beni Mathar–Guefaït Basin likely contributed to the formation of spatially variable, ecologically diverse, and environmentally complex habitats, ranging from open dry grasslands to riparian humid forests. This broad spectrum of habitats created numerous resource-rich microhabitats, providing opportunities for niche diversification and specialisation among mammals, including hominins. The regional mosaic environment, combined with several Green Sahara Periods in the Plio-Pleistocene transition, may have facilitated the dispersal of mammal communities (including hominins) from central or eastern Africa to northern Africa, occupying ecosystems with resource availability similar to their original habitats.

Methods

Permissions, outreach, and engagement

All permits and authorisations for the excavation, sampling and study of the materials involved in this work were granted by the Direction du Patrimoine Culturel, Département de la Culture, Ministère de la Culture et de la Communication du Royaume du Maroc: 2016–2017 Ref. 734/15-06-2016. (Director: Abdellah Alaoui), 2018 Ref. 1121/n17/901/21-07-2017. (Director: Abdellah Alaoui), 2019 Ref. 042/n°1157/01-08-2018 (Director: Youssef Khiara). This Moroccan-Spanish project has carried out several different social and local engagement activities (students and local population) through different activities at the Musée Universitaire d'Archéologie et du Patrimoine (Université Mohammed Premier d'Oujda, BV Mohammed VI B.P. 524 Oujda 60000 Maroc– https://www.ump.ma/fr/musee-universitaire-darcheologie-et-du-patrimoine). Activities include guided visits and open days for (1) secondary school students and their teachers from Oujda and the Oriental region, (2) foreign researchers from various countries and institutions, and (3) teachers of subjects related to archaeology and geology. We have also organised visits to excavations for secondary school students from Jerada, Aïn Béni Mathar and Guefaït, and introductory seminars and training in archaeology for university students from various faculties of the Université Mohammed Premier d'Oujda. The authors affirm that human research participants provided informed consent for publication of the images in Supplementary Fig. 1.

Stable isotope analysis

Stable carbon ($\delta^{13}C$) and oxygen ($\delta^{18}O$) isotope analysis was performed on 11 large vertebrate taxa obtained from GFT-4.2 (Supplementary Fig. 3). Additionally, eight *Hipparion* s. l. teeth were selected for sequential analysis, resulting in the collection of 348 enamel bands for stable oxygen and carbon isotope analyses, 168 for bulk and 180 for sequential analysis (Supplementary Data 1 and 2). Buccal or lingual surfaces were systematically cleaned with a tungsten abrasive drill bit to remove any extraneous material. In *Hipparion* s. l. molars and premolars, the cementum was removed when necessary to access the enamel. Enamel powder for bulk analysis was extracted using a diamond-tipped drill along the entire buccal or lingual surface, following a line from apical to cervical extremities, to ensure the most representative measurement for the whole period of enamel formation. Due to the unknown exact mineralisation period for all the teeth and taxa analysed, we do not rule out the possibility that in this bulk average, we might be capturing part of the signal (some months) associated with the lactation period in some teeth. However, this signal (^{13}C depletion or ^{18}O enrichment) does not seem to be reflected in our results, showing consistent results among all samples analysed from the same taxa.

For sequential samples, we sampled from the crown apex to the enamel-root junction (close to the cervix of the crown). Each sample was a groove measuring 1–2 mm in width, perpendicular to the tooth growth axis, and extending through the thickness of the enamel layer. *Hipparion* s. l. was selected for the sequential analysis due to its pronounced hypsodonty and the well-documented dental development[91]. The permanent cheek teeth mineralisation and eruption sequence for Hipparionini is M_1, M_2, (P_2, P_3), P_4 and M_3[91,92]. Since the M_1 is the first to mineralise and record the signal from maternal milk during the initial months of mineralisation, we avoided sampling this tooth for the sequential analysis. The teeth sampled for GFT-4.2 were: $P_{3/4}$ right, M_3 left, M_2 right, M_3 right, $P^{3/4}$ right, P^3 left, P^4 left, and M^2 left (Supplementary Data 2). The enamel mineralisation period for extant *Equus* is approximately ~30 months for M_2, ~22 months for P_3, ~32 months for P_4, and ~34 months for M_3[93]. However, some studies on Hipparionini based on intra-tooth isotopic analysis suggest a shorter mineralisation period for this genus (~12 months for M_2; ~18 months for P_3; ~24 months for P_4 and M_3)[94,95]. Our intra-tooth analyses support this shorter mineralisation for GFT-4.2 *Hipparion* s. l. teeth, showing sequences likely to span approximately 12–24 months.

Powdered enamel samples weighing between 3.5 to 9.5 mg were chemically treated at the Biomarkers Laboratory of the Institut Català de Paleoecologia Humana i Evolució Social (IPHES-CERCA) using protocols modified from Koch et al.[96] and Tornero et al.[97], wherein samples were treated with 0.1 M acetic acid CH_3COOH (0.1 mL solution/0.1 mg of sample) for 4 h, neutralised with distilled water (5 rinsings), and freeze-dried. The $\delta^{18}O$ and $\delta^{13}C$ values of carbonates were determined using an automated carbonate preparation device (KIEL-III) coupled to a gas-ratio mass spectrometer (Finnigan MAT 252) at the Environmental Isotope Laboratory, University of Arizona, USA. Powdered samples were reacted with dehydrated phosphoric acid under vacuum at 70 °C. The isotope ratio measurement is normalised using a two-point method based on repeated measurements of the calcium carbonate international standards of NBS-19 ($\delta^{18}O = -2.20‰_{VPDB}$, $\delta^{13}C = +1.95‰_{VPDB}$) and NBS-18 ($\delta^{18}O = -23.2 \pm 0.1‰_{VPDB}$, $\delta^{13}C = -5.014 \pm 0.035‰_{VPDB}$) with a precision of ±0.11 ‰ for $\delta^{18}O$ and ±0.08‰ for $\delta^{13}C$ (1 sigma). Samples are typically run in sessions of 46 measurements with precision and normalisation determined for each session. Standards make up 13% of all measurements. Carbon and oxygen isotope composition was reported in δ notation, where $\delta^{13}C$ or $\delta^{18}O = [(R_{sample}/R_{standard}) - 1]$, $R = {}^{13}C/{}^{12}C$ or $^{18}O/^{16}O$, and δ is expressed in per mil, ‰. Carbon and oxygen values were reported relative to the Vienna Pee Dee Belemnite (VPDB) standard.

The cross-correlation analysis was generated using the "ccf" function in R (version 4.4.0) to assess the cross-correlation pattern between the $\delta^{13}C$ and $\delta^{18}O$ intra-tooth analysis and identify different forms of seasonal dietary responses (Supplementary Table 3 and Supplementary Fig. 4). The original R script is available in the following publication[98]. To establish if there were significant differences between the $\delta^{18}O$ values between OD and non-OD taxa from different localities, we conducted a Welch's ANOVA using PAST 4.02[99] after confirming that the samples did not have a normal distribution (normality test) and also lacked homogeneity in variance (Levene's test). The vertebrate faunal list of GFT-4.2 is in Supplementary Table 4.

Dental wear analysis

Dental specimens of ungulates were studied through mesowear and microwear analyses to assess dietary traits. This approach reflects the animal's diet over the months or years before its death (long-term), as mesowear score does not change over short periods such as seasonal variations[100–103]. For the macroscopical mesowear analysis, 60 molars were analysed (Supplementary Data 3). Unworn teeth, highly worn teeth, and those with broken or damaged cusp apices were omitted from mesowear analysis. Cusp sharpness is sensitive to ontogenetic age among young and dentally senescent individuals. However, for intermediate age groups, mesowear is found to be less sensitive to age and more strongly related to diet[104]. Mesowear analysis is a method used to evaluate the relief and sharpness of worn cusp apices in ways that are correlated with the relative amounts of attritional and abrasive wear that they cause on the dental enamel. Mesowear was scored macroscopically from the buccal side of upper molars and the lingual side of lower molars, preferably the sharpest cusp[105]. Additionally, we have utilised teeth ranging from P3 to M3, as proposed by Kaiser and Solounias[106]. A diet with low levels of abrasion, such as browse (high attrition), maintains sharpened apices on the buccal cusps as the tooth wears. In contrast, high levels of abrasion result in more rounded and blunted buccal cusp apices. In this study, the standardised method introduced by Mihlbachler et al.[105] was employed. The method is based on seven cusp categories (0 to 6), ranging in shape from high and sharp (stage 0) to completely blunt with no relief (stage 6). The average value of the individual mesowear data from a single sample corresponds to the mesowear score (MWS). The Fig. 6 was run using PAST 4.02[99].

For the dental microwear analysis, a total of 191 molars and premolars were selected and moulded (Supplementary Data 3). The microwear signal reflects a short-term dietary effect, likely covering the last few days or weeks before death[107]. This signal has been defined as the 'last supper' effect[108]. Therefore, the dental microwear pattern can reveal the animal's diet based on the local and seasonal environmental resources available shortly before death. All moulded specimens were carefully screened under the stereomicroscope, and 86 were discarded from the microwear study due to bad preservation or other taphonomical defects[109–111]. Before moulding, the occlusal surface of each specimen was cleaned using acetone and then 96% ethanol. The surface was moulded using high-resolution and light viscosity silicone (Heraeus Kulzer, PROVIL novo Vinylpolysiloxane, Light C.D. 2 regular set), and transparent casts were created using clear epoxy resin (C.T.S. Spain, EPO 150 + K151). Enamel microwear features were observed via standard light microscopy using a Zeiss Stemi 2000C stereomicroscope at 35× magnification on high-resolution epoxy casts of teeth, following the cleaning, moulding, casting, examination protocol and classification of features defined by Solounias and Semprebon[112] and Semprebon et al.[59]. We used both upper and lower teeth from P4 to M3 according to Xafis et al.[113]. A standard 0.16 mm^2 ocular reticle was employed to quantify the number of small and large pits (round scars), scratches (elongated scars with parallel sides), gouges (irregular edges and much larger and deeper than large pits) and puncture pits (deepest at their centres, symmetrical, crater-like features with regular margins). A quantitative count of total pits and scratches was conducted for the variables mentioned. However, for the remaining variables, a qualitative assessment of presence or absence was performed (1 = presence; 0 = absence). The scratch width score (SWS) is obtained by giving a score of '0' to teeth with predominantly fine scratches per tooth surface, '1' to those with a mixture of fine and coarse types of textures, and '2' to those with predominantly coarse scratches. To achieve a more precise categorisation of grazers, browsers, and mixed feeders, we used the percentage of individuals possessing scratch numbers that fall between 0 and 17 in the 0.16 mm^2 area (0–17%)[114]. The results were compared with a database constructed from extant ungulate taxa[112]. The microwear bivariate graphs (Fig. 7) were generated using the following R script[115].

Plant wax biomarkers

Plant biomarker extraction and isolation. A set of ten samples (GFT 1 to GFT 10) from GFT-4.2 depositional sequence was analysed (see sampling location in Supplementary Fig. 2). Dry, homogenised sediment was subject to pressurised solvent extraction (Büchi Speed Extractor E–916) in three 10 min-cycles in 9:1 (v:v) DCM:MeOH at 100 °C and 103 bar/1500 psi. The solvent containing the total lipid extract (TLE) was concentrated to ~1 mL using a Büchi SyncorePlus evaporator and then evaporated to dryness using a steady stream of N_2 in separate, 4 mL glass vials. The TLE was separated into neutral, acid, and polar fractions by Aminopropyl column chromatography using 4 mL each of 2:1 dichloromethane:isopropanol, 4% acetic acid in diethyl ether, and methanol, respectively. Normal (*n*-) alkanes were isolated from the neutral fraction using silver nitrate-infused silica gel column chromatography with 4 mL hexane.

Molecular characterisation. The *n*-alkanes were analysed with an Agilent 7890B Gas Chromatograph (GC) System equipped with an Agilent HP-5 capillary column (30 m length, 0.25 mm i.d. and 0.25 µm film) and coupled to a 5977A Series Mass Selective Detector (MSD) at the Max Planck Institute of Geoanthropology, Jena, Germany. Samples were injected in pulsed split mode at 290 °C, and the GC oven was programmed from 60 °C (1 min hold) to 150 °C at 10 °C/min, then to 320 °C at 6 °C/min (10 min hold). Helium was the carrier gas with a constant flow of 1.1 mL/min. The MS source was operated at 230 °C with 70 eV ionisation energy in the electron ionisation (EI) mode and a full scan rate of *m/z* 50–650. Plant wax *n*-alkanes were identified by comparing mass spectra and retention times with an external C_{21}-C_{40} standard mixture.

Average chain length (ACL), or the weight-averaged number of carbon homologues of the C_{21}-C_{33} *n*-alkanes, was calculated as follows (Eq. 1):

$$ACL = \frac{21(C_{21}) + 22(C_{22}) + \cdots + 32(C_{32}) + 33(C_{33})}{C_{21} + C_{22} + \cdots + C_{32} + C_{33}} \quad (1)$$

Where C_x is the abundance of the chain length with x carbons.

The carbon preference index (CPI), which examines the odd-over-even carbon number predominance and serves as an indicator for hydrocarbon maturity and degradation[51], was calculated using the abundances of odd and even chain lengths from C_{21} to C_{33} and the following formula (Eq. 2):

$$CPI = \frac{(C_{21} + C_{23} + C_{25} + C_{27} + C_{29} + C_{31}) + (C_{23} + C_{25} + C_{27} + C_{29} + C_{31} + C_{33})}{2 \times (C_{22} + C_{24} + C_{26} + C_{28} + C_{30} + C_{32})} \quad (2)$$

The submerged/terrestrial ratio (STR), which differentiates alkanes produced by either submerged or terrigenous plants, with terrestrial plants generally having values <0.25[54], was calculated as follows (Eq. 3):

$$STR = \frac{C_{25}}{C_{21} + C_{23} + \cdots + C_{31} + C_{31}} \quad (3)$$

The aquatic plant ratio (P_{aq}), which differentiates *n*-alkyl compounds produced by either algae or terrigenous plants, with terrestrial plants generally having values <0.1[53], was calculated as follows (Eq. 4):

$$Paq = \frac{C_{23} + C_{25}}{C_{23} + C_{25} + C_{29} + C_{31}} \quad (4)$$

Compound-Specific Carbon Isotope Analysis. $\delta^{13}C$ values of *n*-alkane homologues C_{25}-C_{31} were measured using an Agilent 7890 A GC System equipped with an Agilent DB-1MS-UI capillary column (60 m length, 0.25 mm i.d. and 0.25 µm film), coupled to a Thermo Fisher Scientific Delta V Plus Isotope Ratio Mass Spectrometer at the Max Planck Institute for Biogeochemistry, Jena, Germany. Samples of 1.0 µL were injected in splitless mode at 320 °C, and the GC oven was maintained for 1 min at an initial temperature of 110 °C before the temperature was increased to 320 °C at 5 °C/min (7 min hold). All the samples were measured in triplicates. Helium was the carrier gas with a constant flow maintained at 1.8 mL/min. We report $\delta^{13}C$ values of C_{25}-C_{31} *n*-alkanes as they were the most abundant in all samples.

The accuracy of the $\delta^{13}C$ values was evaluated against an international standard laboratory mixture (Indiana A7, Arndt Schimmelmann, University of Indiana) injected after every three sample injections. The standard deviation of the C_{16}-C_{30} *n*-alkane working standard was ≤0.5‰ for $\delta^{13}C$. Drift corrections were determined by the standards run after every sample. Carbon isotope composition was reported in δ notation, where $\delta^{13}C = [(R_{sample}/R_{standard}) - 1]$, $R = {}^{13}C/{}^{12}C$, and δ is expressed in per mil, ‰. Carbon values were reported relative to the Vienna Pee Dee Belemnite (VPDB) standard. All mean $\delta^{13}C$ values are reported with their standard deviation.

Finally, linear regression and Spearman's rank test were used to correlate the molecular characterisations of ACL, CPI, and the $\delta^{13}C$ values of the individual C_{25}-C_{31} *n*-alkanes, while Student's *t*-tests and Mann–Whitney *U*-tests were used to test the significance of differences between the C_{25}-C_{31} $\delta^{13}C$ values. These tests were performed after confirming the normal distribution (normality test) and the homogeneity in variance (Levene's test) of our data. All tests were run using PAST 4.03[99] and an Alpha (α) of 0.05.

Pollen analysis

A set of six samples (GFT 1, 2, 4, 6, 8 and 10) from GFT-4.2 depositional sequence was analysed (see sampling location in Supplementary Fig. 2a). Samples were treated with HCl, KOH, concentration with heavy liquid, and a final step with HF[116,117]. Counting was performed with an Olympus Cx41 microscope at 600 magnifications. Fossil pollen and Non-Pollen Palynomorphs (NPP) were identified using published keys[118–125]. Pollen, NPP and microcharcoal concentrations were calculated using the volumetric method (particles/g of dry sediment) described in refs. 117,126.

Small vertebrates

The small vertebrate material referred to here was recovered from sediment collected at the GFT-4 site, including GFT-4.2 locality (Supplementary Fig. 2a), during the excavation campaigns of 2017 and 2018. All sediment was water-screened using superimposed 4-, 1- and 0.5-mm mesh sieves. The collection from GFT-4 includes 330 rodent teeth corresponding to nine different taxa and 47 disarticulated cranial and postcranial bones of amphibians and squamates comprising at least five taxa. The vertebrate faunal list of GFT-4.2 is in Supplementary Table 4.

Micro-crustaceans and algae remains

Three sediment samples (GFT 1, 3 and 5 (GFT 5 is a sterile sample); see sampling location in Supplementary Fig. 2a) of 70–120 g from the GFT-4.2 section were disaggregated by treatment with 3% H_2O_2 for 48 h. The material was washed through 100-μm, 250-μm and 1000-μm sieves, dried, and calcareous remains picked from sieve residues under a low-power binocular Olympus SZ60 microscope. A Hitachi TM3000 scanning electron microscope was used for ostracod-valve documentation and to support identification, which was mostly based on the key for the modern Algerian fauna[127], and western and central European fauna[128].

Digital mapping

Digital terrain model source was carried out using ArcGIS 10.8 software (ETOPO2 (NGDC)), available at the Digital Mapping and 3D Analysis Laboratory (CENIEH, Spain) and TanDEM-X (DLR).

Reporting summary

Further information on research design is available in the Nature Portfolio Reporting Summary linked to this article.

Data availability

All data generated or analysed during this study are included in this published article (and its supplementary information files). Original fossils are housed at the Musée Universitaire d'Archéologie et du Patrimoine at the Université Mohammed Premier (Oujda, Morocco). The source data for Figs. 2–8 and Supplementary Figs. 4 and 5 are provided as a Source Data file. Source data are provided with this paper.

Code availability

No code has been created for this study. The R scripts used are based on previously published data, which are available in the references.

References

1. Kingston, J. D. & Harrison, T. Isotopic dietary reconstructions of Pliocene herbivores at Laetoli: implications for early hominin paleoecology. *Palaeogeogr. Palaeoclimatol. Palaeoecol.* **243**, 272–306 (2007).
2. Ségalen, L., Lee-Thorp, J. A. & Cerling, T. Timing of C_4 grass expansion across sub-Saharan Africa. *J. Hum. Evol.* **53**, 549–559 (2007).
3. Levin, N. E., Simpson, S. W., Quade, J., Cerling, T. E. & Frost, S. R. Herbivore enamel carbon isotopic composition and the environmental context of *Ardipithecus* at Gona, Ethiopia. *Spec. Pap. Geol. Soc. Am.* **446**, 215–235 (2008).
4. Bedaso, Z. K., Wynn, J. G., Alemseged, Z. & Geraads, D. Dietary and paleoenvironmental reconstruction using stable isotopes of herbivore tooth enamel from middle Pliocene Dikika, Ethiopia: implication for *Australopithecus afarensis* habitat and food resources. *J. Hum. Evol.* **64**, 21–38 (2013).
5. Cerling, T. E. et al. Dietary changes of large herbivores in the Turkana Basin, Kenya, from 4 to 1 Ma. *Proc. Natl Acad. Sci. USA* **112**, 11467–11472 (2015).
6. Robinson, J. R., Rowan, J., Campisano, C. J., Wynn, J. G. & Reed, K. E. Late Pliocene environmental change during the transition from *Australopithecus* to *Homo*. *Nat. Ecol. Evol.* **1**, 1–7 (2017).
7. Robinson, J. R., Rowan, J., Barr, W. A. & Sponheimer, M. Intrataxonomic trends in herbivore enamel $\delta^{13}C$ are decoupled from ecosystem woody cover. *Nat. Ecol. Evol.* **5**, 995–1002 (2021).
8. Lüdecke, T. et al. Dietary versatility of Early Pleistocene hominins. *Proc. Natl Acad. Sci. USA* **115**, 13330–13335 (2018).
9. Lee-Thorp, J. et al. Isotopic evidence for an early shift to C_4 resources by Pliocene hominins in Chad. *Proc. Natl Acad. Sci. USA* **109**, 20369–20372 (2012).
10. Zazzo, A. et al. Herbivore paleodiet and paleoenvironmental changes in Chad during the Pliocene using stable isotope ratios of tooth enamel carbonate. *Paleobiology* **26**, 294–309 (2000).
11. Lee-Thorp, J. A. & Sponheimer, M. Opportunities and constraints for reconstructing palaeoenvironments from stable light isotope ratios in fossils. *Geol. Q.* **49**, 195–203 (2005).
12. Lee-Thorp, J. A., Sponheimer, M. & Luyt, J. Tracking changing environments using stable carbon isotopes in fossil tooth enamel: an example from the South African hominin sites. *J. Hum. Evol.* **53**, 595–601 (2007).
13. Lee-Thorp, J. A., Sponheimer, M., Passey, B. H., De Ruiter, D. J. & Cerling, T. E. Stable isotopes in fossil hominin tooth enamel suggest a fundamental dietary shift in the Pliocene. *Philos. Trans. R. Soc. B Biol. Sci.* **365**, 3389–3396 (2010).
14. Lehmann, S. B. et al. Stable isotopic composition of fossil mammal teeth and environmental change in southwestern South Africa during the Pliocene and Pleistocene. *Palaeogeogr. Palaeoclimatol. Palaeoecol.* **457**, 396–408 (2016).
15. Sahnouni, M. et al. 1.9-million- and 2.4-million-year-old artifacts and stone tool–cutmarked bones from Ain Boucherit, Algeria. *Science* **362**, 1297–1301 (2018).
16. Cáceres, I. et al. Assessing the subsistence strategies of the earliest North African inhabitants: evidence from the Early Pleistocene site of Ain Boucherit (Algeria). *Archaeol. Anthropol. Sci.* **15**, 87 (2023).
17. Gallotti, R. et al. First high resolution chronostratigraphy for the early North African Acheulean at Casablanca (Morocco). *Sci. Rep.* **11**, 1–14 (2021).
18. Sala-Ramos, R. et al. Pleistocene and Holocene peopling of Jerada province, eastern Morocco: introducing a research project. Le peuplement humain pendant le Pléistocène et l'Holocène dans la province de Jerada, Maroc oriental: introduction d'un projet de recherche. *Bull. d'Archéol. Marocaine* **27**, 27–40 (2022).
19. Larrasoaña, J. C., Roberts, A. P. & Rohling, E. J. Dynamics of Green Sahara Periods and their role in hominin evolution. *PLoS ONE* **8**, e76514 (2013).
20. Larrasoaña, J. C. A review of West African monsoon penetration during Green Sahara Periods; implications for human evolution and dispersals over the last three million years. *Oxford Open Clim. Chang.* **1**, 1–19 (2021).
21. Trauth, M. H., Larrasoaña, J. C. & Mudelsee, M. Trends, rhythms and events in Plio-Pleistocene African climate. *Quat. Sci. Rev.* **28**, 399–411 (2009).
22. Trauth, M. H. et al. Northern Hemisphere Glaciation, African climate and human evolution. *Quat. Sci. Rev.* **268**, 107095 (2021).
23. Hennissen, J. A. I., Head, M. J., De Schepper, S. & Groeneveld, J. Dinoflagellate cyst paleoecology during the Pliocene–Pleistocene climatic transition in the North Atlantic. *Palaeogeogr. Palaeoclimatol. Palaeoecol.* **470**, 81–108 (2016).
24. Grant, K. M. et al. Organic carbon burial in Mediterranean sapropels intensified during Green Sahara Periods since 3.2 Myr ago. *Commun. Earth Environ.* **3**, 1–9 (2022).
25. Cohen, A. S. et al. Plio-Pleistocene environmental variability in Africa and its implications for mammalian evolution. *Proc. Natl Acad. Sci. USA* **119**, 1–7 (2022).

26. Patalano, R. et al. Microhabitat variability in human evolution. *Front. Earth Sci.* **9**, 1–19 (2021).
27. Parés, J. et al. First magnetostratigraphic results in the Aïn Beni Mathar-Guefaït Basin, Northern High Plateaus (Morocco): the Pliocene-Pleistocene Dhar Iroumyane composite section. *Geobios* **76**, 17–36 (2023).
28. Ramírez-Pedraza, I. et al. Multiproxy approach to reconstruct fossil primate feeding behavior: case study for macaque from the Plio-Pleistocene site Guefaït-4.2 (eastern Morocco). *Front. Ecol. Evol.* **11**, 1011208 (2023).
29. Lee-Thorp, J., Thackeray, J. F. & van der Merwe, N. The hunters and the hunted revisited. *J. Hum. Evol.* **39**, 565–576 (2000).
30. Lee-Thorp, J. A., Sealy, J. C. & van der Merwe, N. J. Stable carbon isotope ratio differences between bone collagen and bone apatite, and their relationship to diet. *J. Archaeol. Sci.* **16**, 585–599 (1989).
31. Sillen, A. & Lee-Thorp, J. A. Trace element and isotopic aspects of predator-prey relationships in terrestrial foodwebs. *Palaeogeogr. Palaeoclimatol. Palaeoecol.* **107**, 243–255 (1994).
32. Levin, N. E., Cerling, T. E., Passey, B. H., Harris, J. M. & Ehleringer, J. R. A stable isotope aridity index for terrestrial environments. *Proc. Natl Acad. Sci. USA* **103**, 11201–11205 (2006).
33. Blumenthal, S. A. et al. Aridity and hominin environments. *Proc. Natl Acad. Sci. USA* **114**, 7331–7336 (2017).
34. Roberts, P. et al. Fossil herbivore stable isotopes reveal middle Pleistocene hominin palaeoenvironment in 'Green Arabia'. *Nat. Ecol. Evol.* **2**, 1871–1878 (2018).
35. Faith, J. T. Paleodietary change and its implications for aridity indices derived from $\delta^{18}O$ of herbivore tooth enamel. *Palaeogeogr. Palaeoclimatol. Palaeoecol.* **490**, 571–578 (2018).
36. Kohn, M. J. Predicting animal $\delta^{18}O$: accounting for diet and physiological adaptation. *Geochim. Cosmochim. Acta* **60**, 4811–4829 (1996).
37. Kohn, M. J., Schoeninger, M. & Valley, J. W. Herbivore tooth oxygen isotope compositions: effect of diet and physiology. *Geochim. Cosmochim. Acta* **60**, 3889–3896 (1996).
38. Belsky, A. J. et al. The effects of trees on their physical, chemical and biological environments in a semi-arid savanna in Kenya. *J. Appl. Ecol.* **26**, 1005–1024 (1989).
39. Ramírez-Pedraza, I. et al. Palaeoecological reconstruction of Plio-Pleistocene herbivores from the Ahl al Oughlam site (Casablanca, Morocco): insights from dental wear and stable isotopes. *Quat. Sci. Rev.* **319**, 108341 (2023).
40. Liu, W., Yang, H. & Li, L. Hydrogen isotopic compositions of *n*-alkanes from terrestrial plants correlate with their ecological life forms. *Oecologia* **150**, 330–338 (2006).
41. Hou, J., D'Andrea, W. J., MacDonald, D. & Huang, Y. Evidence for water use efficiency as an important factor in determining the δD values of tree leaf waxes. *Org. Geochem.* **38**, 1251–1255 (2007).
42. Dodd, R. S. & Poveda, M. M. Environmental gradients and population divergence contribute to variation in cuticular wax composition in *Juniperus communis*. *Biochem. Syst. Ecol.* **31**, 1257–1270 (2003).
43. Castañeda, I. S., Werne, J. P., Johnson, T. C. & Filley, T. R. Late Quaternary vegetation history of southeast Africa: the molecular isotopic record from Lake Malawi. *Palaeogeogr. Palaeoclimatol. Palaeoecol.* **275**, 100–112 (2009).
44. Duan, Y. & He, J. Distribution and isotopic composition of *n*-alkanes from grass, reed and tree leaves along a latitudinal gradient in China. *Geochem. J.* **45**, 199–207 (2011).
45. Carr, A. S. et al. Leaf wax *n*-alkane distributions in arid zone South African flora: environmental controls, chemotaxonomy and palaeoecological implications. *Org. Geochem.* **67**, 72–84 (2014).
46. Bush, R. T. & McInerney, F. A. Influence of temperature and C_4 abundance on *n*-alkane chain length distributions across the central USA. *Org. Geochem.* **79**, 65–73 (2015).
47. Bray, E. E. & Evans, E. D. Distribution of *n*-paraffins as a clue to recognition of source beds. *Geochim. Cosmochim. Acta* **22**, 2–15 (1961).
48. Castañeda, I. S. & Schouten, S. A review of molecular organic proxies for examining modern and ancient lacustrine environments. *Quat. Sci. Rev.* **30**, 2851–2891 (2011).
49. Diefendorf, A. F., Freeman, K. H., Wing, S. L. & Graham, H. V. Production of *n*-alkyl lipids in living plants and implications for the geologic past. *Geochim. Cosmochim. Acta* **75**, 7472–7485 (2011).
50. Jaeschke, A. et al. Influence of land use on distribution of soil *n*-alkane δD and brGDGTs along an altitudinal transect in Ethiopia: implications for (paleo)environmental studies. *Org. Geochem.* **124**, 77–87 (2018).
51. Duan, Y. & Xu, L. Distributions of *n*-alkanes and their hydrogen isotopic composition in plants from Lake Qinghai (China) and the surrounding area. *Appl. Geochem.* **27**, 806–814 (2012).
52. Jha, D. K. et al. Preservation of plant-wax biomarkers in deserts implications for Quaternary environment and human evolutionary studies. *J. Quat. Sci*. **39**, 349–358 (2024).
53. Ficken, K. J., Li, B., Swain, D. L. & Eglinton, G. An *n*-alkane proxy for the sedimentary input of submerged/floating freshwater aquatic macrophytes. *Org. Geochem.* **31**, 745–749 (2000).
54. Liu, H. & Liu, W. Concentration and distributions of fatty acids in algae, submerged plants and terrestrial plants from the northeastern Tibetan Plateau. *Org. Geochem.* **113**, 17–26 (2017).
55. Van Geel, B. A palaeoecological study of Holocene peat bog sections in Germany and The Netherlands, based on the analysis of pollen, spores and macro and microscopic remains of fungi, algae, cormophytes and animals. *Rev. Palaeobot. Palynol.* **25**, 1–120 (1978).
56. Benito-Calvo, A. et al. Geomorphological analysis using small unmanned aerial vehicles and submeter GNSS (Gara Soultana butte, High Plateaus Basin, Eastern Morocco). *J. Maps* **16**, 459–467 (2020).
57. Parés, J. et al. Magnetostratigraphy of the sedimentary fill of the Aïn Beni Mathar-Guefaït Basin (High Plateau, E Morocco). In *Proc. 2020 AGU Fall Meeting* (2020).
58. Escoriza, D. & Comas, M. Is *Hyalosaurus koellikeri* a true forest lizard? *Herpetol. Conserv. Biol.* **10**, 610–620 (2015).
59. Semprebon, G. M., Godfrey, L. R., Solounias, N., Sutherland, M. R. & Jungers, W. L. Can low-magnification stereomicroscopy reveal diet? *J. Hum. Evol.* **47**, 115–144 (2004).
60. Godfrey, L. R. et al. Dental use wear in extinct lemurs: evidence of diet and niche differentiation. *J. Hum. Evol.* **47**, 145–169 (2004).
61. Piñero, P. et al. *Golunda aouraghei*, sp. nov., the last representative of the genus *Golunda* in Africa. *J. Vertebr. Paleontol.* **39**, 1–6 (2020).
62. Aulagnier, S. et al. *Eliomys melanurus* (amended version of 2016 assessment). *IUCN Red List of Threatened Species 2021 e.T7619A197505035*. https://doi.org/10.2305/IUCN.UK.2021-1.RLTS.T7619A197505035.en (2021).
63. Amori, G., Hutterer, R., Kryštufek, B. & Yigit, N. *Eliomys munbyanus*. *IUCN Red List of Threatened Species 2022 e.T136469A22223369*. https://doi.org/10.2305/IUCN.UK.2022-2.RLTS.T136469A22223369.en (2022).
64. Zhou, H., Helliker, B. R., Huber, M., Dicks, A. & Akçay, E. C_4 photosynthesis and climate through the lens of optimality. *Proc. Natl Acad. Sci. USA* **115**, 12057–12062 (2018).
65. Cassola, F. *Ctenodactylus gundi*. *IUCN Red List of Threatened Species 2022 e.T5792A22191625*. https://doi.org/10.2305/IUCN.UK.2022-2.RLTS.T5792A22191625.en (2022).

66. De Bruijn, H. Superfamily Sciuroidea in *The Miocene Land Mammals of Europe* (eds Rössner, G. E. & Heissig, K.) 271–280 (Dr. Friedrich Pfeil, 1999).
67. Kryštufek, B., Mahmoudi, A., Tesakov, A. S., Matějů, J. & Hutterer, R. A review of bristly ground squirrels Xerini and a generic revision in the African genus *Xerus*. *Mammalia* **80**, 521–540 (2016).
68. Pausas, J. G. Changes in fire climate in the easter Iberian Peninsula (Mediterranean Basin). *Clim. Change* **63**, 337–350 (2004).
69. Bunting, M. J., Gaillard, M. J., Sugita, S., Middleton, R. & Broström, A. Vegetation structure and pollen source area. *Holocene* **14**, 651–660 (2004).
70. Domingo, L. et al. Late Neogene and Early Quaternary paleoenvironmental and paleoclimatic conditions in Southwestern Europe: isotopic analyses on mammalian taxa. *PLoS ONE* **8**, e63739 (2013).
71. Szabó, P. et al. Pliocene–Early Pleistocene continental climate and vegetation in Europe based on stable isotope compositions of mammal tooth enamel. *Quat. Sci. Rev.* **288**, 107572 (2022).
72. Bocherens, H., Koch, P. L., Mariotti, A., Geraads, D. & Jaeger, J. J. Isotopic biogeochemistry (^{13}C, ^{18}O) of mammalian enamel from African Pleistocene hominid sites. *Palaios* **11**, 306–318 (1996).
73. Fannin, L. D. et al. Carbon and strontium isotope ratios shed new light on the paleobiology and collapse of *Theropithecus*, a primate experiment in graminivory. *Palaeogeogr. Palaeoclimatol. Palaeoecol.* **572**, 110393 (2021).
74. Duval, M. et al. The Plio-Pleistocene sequence of Oued Boucherit (Algeria): a unique chronologically-constrained archaeological and palaeontological record in North Africa. *Quat. Sci. Rev.* **271**, 107116 (2021).
75. Ungar, P. S. & Sponheimer, M. The diets of early hominins. *Science* **334**, 190–193 (2011).
76. Levin, N. E., Haile-Selassie, Y., Frost, S. R. & Saylor, B. Z. Dietary change among hominins and cercopithecids in Ethiopia during the early Pliocene. *Proc. Natl Acad. Sci. USA* **112**, 12304–12309 (2015).
77. Wynn, J. G. et al. Isotopic evidence for the timing of the dietary shift toward C_4 foods in eastern African *Paranthropus*. *Proc. Natl Acad. Sci. USA* **117**, 21978–21984 (2020).
78. Lebatard, A. E. et al. Cosmogenic nuclide dating of *Sahelanthropus tchadensis* and *Australopithecus bahrelghazali*: Mio-Pliocene hominids from Chad. *Proc. Natl Acad. Sci. USA* **105**, 3226–3231 (2008).
79. Stewart, K. M. Environmental change and hominin exploitation of C_4-based resources in wetland/savanna mosaics. *J. Hum. Evol.* **77**, 1–16 (2014).
80. Zeller, E. et al. Human adaptation to diverse biomes over the past 3 million years. *Science* **380**, 604–608 (2023).
81. Dart, R. *Australopithecus africanus*: the man-ape of South Africa. *Nature* **115**, 195–199 (1925).
82. Coppens, Y. East side story: the origin of humankind. *Sci. Am.* **270**, 88–95 (1994).
83. Potts, R. Environmental hypotheses of hominin evolution. *Yearb. Phys. Anthropol.* **41**, 93–136 (1998).
84. Lupien, R. L. et al. A leaf wax biomarker record of early Pleistocene hydroclimate from West Turkana, Kenya. *Quat. Sci. Rev.* **186**, 225–235 (2018).
85. Mercader, J. et al. Earliest Olduvai hominins exploited unstable environments ~ 2 million years ago. *Nat. Commun.* **12**, 3 (2021).
86. Plummer, T. W. et al. Expanded geographic distribution and dietary strategies of the earliest Oldowan hominins and *Paranthropus*. *Science* **566**, 561–566 (2023).
87. Potts, R. et al. Increased ecological resource variability during a critical transition in hominin evolution. *Sci. Adv.* **6**, 1–15 (2020).
88. Foister, T., Tallavaara, M., Fortelius, M. & Wilson, O. E. Homo heterogenus: variability in Pleistocene *Homo* environments. *Evol. Anthropol.* **32**, 373–385 (2023).
89. Peppe, D. J. et al. Oldest evidence of abundant C_4 grasses and habitat heterogeneity in eastern Africa. *Science* **380**, 173–177 (2023).
90. Maslin, M. A. et al. East african climate pulses and early human evolution. *Quat. Sci. Rev.* **101**, 1–17 (2014).
91. Orlandi-Oliveras, G., Nacarino-Meneses, C. & Köhler, M. Dental histology of late Miocene hipparionins compared with extant *Equus*, and its implications for Equidae life history. *Palaeogeogr. Palaeoclimatol. Palaeoecol.* **528**, 133–146 (2019).
92. Domingo, M. S. et al. First radiological study of a complete dental ontogeny sequence of an extinct Equid: implications for Equidae life history and taphonomy. *Sci. Rep.* **8**, 1–11 (2018).
93. Hoppe, K. A., Stover, S. M., Pascoe, J. R. & Amundson, R. Tooth enamel biomineralization in extant horses: implications for isotopic microsampling. *Palaeogeogr. Palaeoclimatol. Palaeoecol.* **206**, 355–365 (2004).
94. Nelson, S. V. Paleoseasonality inferred from equid teeth and intratooth isotopic variability. *Palaeogeogr. Palaeoclimatol. Palaeoecol.* **222**, 122–144 (2005).
95. van Dam, J. A. & Reichart, G. J. Oxygen and carbon isotope signatures in late Neogene horse teeth from Spain and application as temperature and seasonality proxies. *Palaeogeogr. Palaeoclimatol. Palaeoecol.* **274**, 64–81 (2009).
96. Koch, P. L., Tuross, N. & Fogel, M. L. The effects of sample treatment and diagenesis on the isotopic integrity of carbonate in biogenic hydroxylapatite. *J. Archaeol. Sci.* **24**, 417–429 (1997).
97. Tornero, C., Bălăşescu, A., Ughetto-Monfrin, J., Voinea, V. & Balasse, M. Seasonality and season of birth in early Eneolithic sheep from Cheia (Romania): methodological advances and implications for animal economy. *J. Archaeol. Sci.* **40**, 4039–4055 (2013).
98. Yang, D. et al. Intra-tooth stable isotope analysis reveals seasonal dietary variability and niche partitioning among bushpigs/red river hogs and warthogs. *Curr. Zool.* https://doi.org/10.1093/cz/zoae007 (2024).
99. Hammer, Ø., Harper, D. A. & Ryan, P. D. Past: paleontological statistics software package for education and data analysis. *Palaeontol. Electron.* **4**, 5–7 (2001).
100. Kaiser, T. M. & Schulz, E. Tooth wear gradients in zebras as an environmental proxy—a pilot study. *Mitt. Hamb. Zool. Mus. Inst.* **103**, 187–211 (2006).
101. Rivals, F. & Solounias, N. Differences in tooth microwear of populations of caribou (*Rangifer tarandus*, Ruminantia, Mammalia) and implications to ecology, migration, glaciations and dental evolution. *J. Mamm. Evol.* **14**, 182–192 (2007).
102. Solounias, N., Tariq, M., Hou, S., Danowitz, M. & Harrison, M. A new method of tooth mesowear and a test of it on domestic goats. *Ann. Zool. Fenn.* **51**, 111–118 (2014).
103. Ackermans, N. L. et al. Dental wear proxy correlation in a long-term feeding experiment on sheep (*Ovis aries*). *J. R. Soc. Interface* **18**, 20210139 (2021).
104. Rivals, F., Mihlbachler, M. C. & Solounias, N. Effect of ontogenetic-age distribution in fossil and modern samples on the interpretation of ungulate paleodiets using the mesowear method. *J. Vertebr. Paleontol.* **27**, 763–767 (2007).
105. Mihlbachler, M. C., Rivals, F., Solounias, N. & Semprebon, G. M. Dietary change and evolution of horses in North America. *Science* **331**, 1178–1181 (2011).
106. Franz-Odendaal, T. A. & Kaiser, T. M. Differential mesowear in the maxillary and mandibular cheek dentition of some ruminants (Artiodactyla). *Ann. Zool. Fenn.* **40**, 395–410 (2003).

107. Teaford, M. F. & Oyen, O. J. Differences in the rate of molar wear between monkeys raised on different diets. *J. Dent. Res.* **68**, 1513–1518 (1989).
108. Grine, F. E. Dental evidence for dietary differences in *Australopithecus* and *Paranthropus*: a quantitative analysis of permanent molar microwear. *J. Hum. Evol.* **15**, 783–822 (1986).
109. King, T., Andrews, P. & Boz, B. Effect of taphonomic processes on dental microwear. *Am. J. Phys. Anthropol.* **108**, 359–373 (1999).
110. Micó, C. et al. Differentiating taphonomic features from trampling and dietary microwear, an experimental approach. *Hist. Biol.* **00**, 1–23 (2023).
111. Uzunidis, A. et al. The impact of sediment abrasion on tooth microwear analysis: an experimental study. *Archaeol. Anthropol. Sci.* **13**, 1–17 (2021).
112. Solounias, N. & Semprebon, G. M. Advances in the reconstruction of ungulate ecomorphology with application to early fossil equids. *Am. Museum Novit.* **3366**, 1–49 (2002).
113. Xafis, A., Nagel, D. & Bastl, K. Which tooth to sample? A methodological study of the utility of premolar/non-carnassial teeth in the microwear analysis of mammals. *Palaeogeogr. Palaeoclimatol. Palaeoecol.* **487**, 229–240 (2017).
114. Semprebon, G. M. & Rivals, F. Was grass more prevalent in the pronghorn past? An assessment of the dietary adaptations of Miocene to Recent Antilocapridae (Mammalia: Artiodactyla). *Palaeogeogr. Palaeoclimatol. Palaeoecol.* **253**, 332–347 (2007).
115. Rivals, F. MicrowearBivaR: a code to create tooth microwear bivariate plots in R (Versión 1). Zenodo https://doi.org/10.5281/zenodo.2587575 (2019).
116. Goeury, C. & de Beaulieu, J. L. À propos de la concentration du pollen à l'aide de la liqueur de Thoulet dans les sédiments minéraux. *Pollen Spores* **21**, 239–251 (1979).
117. Burjachs, F., López Sáez, J. A. & Iriarte, M. J. Metodología arqueopalinológica in *La Recogida de Muestras en Arqueobotànica: Objetivos y Propuestas Metodológicas* (eds Buxó, R. & Piqué, R.) 9–16 (Museu d'Arqueologia de Catalunya, 2003).
118. Käärik, A., Keller, J., Kiffer, E., Perreau, J. & Reisinger, O. *Atlas of Airborne Fungal Spores in Europe* (Springer, 1983).
119. Jarzen, D. M. & Elsik, W. C. Fungal palynomorphs recovered from recent river deposits, Luangwa Valley, Zambia. *Palynology* **10**, 35–60 (1986).
120. Van Geel, B. The application of fungal and algal remains and other microfossils in palynological analyses in *Handbook of Holocene Palaeoecology and Palaeohydrology* (ed. Berglund, B. E.) 497–505 (Wiley, 1986).
121. Moore, P. D., Webb, J. A. & Collinson, M. E. *Pollen Analysis* (Blackwell, 1991).
122. Reille, M. *Pollen et Spores d'Europe et d'Afrique du Nord* (Laboratoire de Botanique Historique et Palynologie, 1992).
123. Reille, M. *Pollen et spores d'Europe et d'Afrique du Nord (Supplément 1)* (Laboratoire de Botanique Historique et Palynologie, 1995).
124. Davis, O. K. & Shafer, D. S. *Sporormiella* fungal spores, a palynological means of detecting herbivore density. *Palaeogeogr. Palaeoclimatol. Palaeoecol.* **237**, 40–50 (2006).
125. Miola, A. Tools for non-pollen palynomorphs (NPPs) analysis: a list of Quaternary NPP types and reference literature in English language (1972–2011). *Rev. Palaeobot. Palynol.* **186**, 142–161 (2012).
126. Loublier, Y. *Application de l'Analyse Pollinique à l'Étude du Paléoenvironnement du Remplissage Würmien de la Grotte de L'Arbreda (Espagne)*. PhD dissertation, Université des Sciences e Techniques du Languedoc (1978).
127. Menail, A., Scharf, B. & Amarouayache, M. Living ostracods (Crustacea) from Algerian Sahara and High Plains: ecological data and new records. *Zootaxa* **5227**, 501–530 (2023).
128. Meisch, C. *Freshwater Ostracoda of Western and Central Europe (Süswasserfauna von Mitteleuropa)* (Spektrum, 2000).
129. Fortelius, M. & Solounias, N. Functional characterization of ungulate molars using the abrasion-attrition wear gradient: a new method for reconstructing paleodiets. *Am. Museum Novit.* **3301**, 1–36 (2000).

Acknowledgements

We express our gratitude to the Jerada Government and Local Authorities of Aïn Beni Mathar and Guefaït for providing local permits for conducting geological, archaeological, and palaeontological fieldwork in the region and to the local population for their support, collaboration, and help. We also want to acknowledge the German Aerospace Center for granting permission (DEM GEOL 3286) to use TanDEM-X data. Funding for this research was provided by: Spanish Ministry of Culture and Sport (Ref: 40-T002018N0000042853 & 170-T002019N0000038589), Faculty of Sciences (Mohamed 1r University of Oujda, Morocco), Palarq Foundation, Direction of Cultural Heritage (Ministry of Culture and Communication, Morocco), Faculty of Sciences (Université Mohammed Premier of Oujda, Morocco), INSAP (Institut National des Sciences de l'Archéologie et du Patrimoine), Spanish Ministry of Science, Innovation and Universities (Grant PID2021-123092NB-C21 funded by MCIN/AEI/10.13039/501100011033 and by "ERDF A way of making Europe"), Research Groups Support of the Catalonia Government (2021 SGR 01238-2023PFR-URV-01238 (URV) Palhum (AGAUR) and 2021 SGR 01237 GAPS (AGAUR)-2023PFR-URV-01237 (URV)). C.T. is supported by the Spanish Ministry of Science and Innovation through the "Ramón y Cajal" (RYC2020-029404-I). A.R.-H. is supported by the Spanish Ministry of Science, Innovation, and Universities through the "Ramón y Cajal" (RYC2022-037802-I). J.v.d.M. is supported by PID2021-122355NB-C33 financed by MCIN/AEI/10.13039/501100011033/FEDER. P.P. is supported by the "Juan de la Cierva-Incorporación" contract (grant IJC2020-044108-I) funded by MCIN/AEI/10.13039/501100011033 and "European Union Next Generation EU/PRTR". H.-A.B. has been supported by project PID2021-122533NB-I00 (Spanish Ministry of Science and Innovation). C.S.-B. is supported by a FPI Predoctoral Scholarship (PRE2020-094482) associated with project CEX2019-000945-M-20-1 with the financial sponsorship of the Spanish Ministry of Science and Innovation. P.R. and D.K.J. would like to thank the Max Planck Society for funding and support. The Institut Català de Paleoecologia Humana i Evolució Social (IPHES-CERCA) has received financial support from the Spanish Ministry of Science and Innovation through the "María de Maeztu" program for Units of Excellence (CEX2019-000945-M). R.S.-R., M.G.C.H., F.R., I.E., P.P. and H.-A.B. research is funded by CERCA Programme/Generalitat de Catalunya.

Author contributions

I.R.-P. conceived and designed this research. A.A., A.R.-H., J.v.d.M., H.A., A.O., A.L., J.A., P.P., H.H., C.S.-B., I.R.-P., A.B.-C., H.M., E.M.-R., M.S., R.S.-R. and M.G.C.H. participated in the fieldwork and provided materials and background for the research. A.R.-H., H.A., and J.v.d.M. identified the macrofaunal remains. A.R.-H. supervised the excavation. I.R.-P. and C.T. conducted the stable isotope analysis in faunal remains. I.E. conducted the pollen analysis. I.R.-P. and F.R. performed the dental wear analysis. S.M. conducted the microcrustaceans and algae analysis. P.P. and J.A. carried out the analysis of the rodent remains. H.-A.B., and C.S.-B. carried out the analysis of the herpetofauna remains. R.P., P.R., D.K.J., and I.R.-P. performed the plant wax biomarkers analysis. A.B.-C. conducted the mapping and the stratigraphic section. M.G.CH., R.S.-R. and H.A. are the principal investigators of the project and are responsible for project research objectives, administration and funding acquisition. I.R.-P. wrote the paper with input from all authors.

Competing interests

The authors declare no competing interests.

Additional information

Supplementary information The online version contains supplementary material available at https://doi.org/10.1038/s41467-024-52672-0.

Correspondence and requests for materials should be addressed to Iván Ramírez-Pedraza.

Peer review information *Nature Communications* thanks Antoine Souron and the other anonymous reviewer(s) for their contribution to the peer review of this work. A peer review file is available.